



**COMOTI**  
ROMANIAN RESEARCH &  
DEVELOPMENT INSTITUTE FOR  
GAS TURBINES

# TURBO

Scientific Journal

vol. IX (2022), no. 2

# Order of Cultural Merit in Knight rank, Category H - Scientific research,

Mrs. Dimitriu Delia-Gabriela,

Doctor, Research Professor,  
Manchester Metropolitan University and  
Researcher at NRDl for Gas Turbines COMOTI.



SCIENCE  
RESEARCH

Congratulation Delia!

COMOTI is  
proud of you!



**PRESIDENT:**

Dr. Eng. Valentin SILIVESTRU

**VICE-PRESIDENT:**

Dr. Eng. Romulus PETCU  
Dr. Eng. Cristian CARLANESCU

**TECHNICAL SECRETARY:**

Dr. Eng. Jeni VILAG

**MEMBERS:**

Prof. Dr. Virgil STANCIU  
Prof. Dr. Corneliu BERBENTE  
Prof. Dr. Dan ROBESCU  
Prof. Dr. Sterian DANAILA  
Conf. Dr. Eng. Daniel-Eugeniu CRUNTEANU  
Conf. Dr. Eng. Grigore CICAN  
Mat. Dr. Eng. Catalin NAE  
Dr. Eng. Gheorghe MATACHE  
Dr. Eng. Ene BARBU  
Dr. Eng. Gheorghe FETEA  
Dr. Eng. Valeriu VILAG  
Dr. Eng. Ionuț PORUMBEL  
Dr. Eng. Valeriu DRAGAN  
Dr. Eng. Lucia Raluca MAIER  
Dr. Eng. Andreea MANGRA  
Dr. Eng. Sorin GABROVEANU

**EDITOR IN CHIEF:**

Prof. Dr. Lacramioara ROBESCU

**EDITORS:**

Dr. Eng. Mihaela Raluca CONDRUZ  
Ec. Elena BANEA

**ADMINISTRATIVE SECRETARY:**

Eng. Mihaela GRIGORESCU

**TRANSLATION CHECKING:**

Dr. Eng. Ionuț PORUMBEL  
Oana HRITCU

**GRAPHICS:**

Victor BESLEAGA

More information:

[http://www.comoti.ro/ro/jurnalul\\_stiintific\\_turbo.htm](http://www.comoti.ro/ro/jurnalul_stiintific_turbo.htm)  
[jeni.vilag@comoti.ro](mailto:jeni.vilag@comoti.ro)

ISSN: 2559-608X

ISSN-L: 1454-2897

Scientific Journal TURBO is included in the following international databases:

-ICI World of Journals:

ICV 2021: 83,53

<https://journals.indexcopernicus.com/search/details?id=48512>

-Directory of Open Access Scholarly Resources (ROAD)

<https://portal.issn.org/resource/ISSN/2559-608X#>

-Directory of Research Journals Indexing (DRJI):

<http://olddrji.lbp.world/JournalProfile.aspx?jid=2559-608X>

♦ Editorial .....2

TECHNOLOGIES :

♦ Intelligent crossing for reducing traffic jams  
R. Stoica, M. Roman, D. Lale.....4

MATERIALS AND TECHNOLOGIES :

♦ Physical and mathematical model of the electric drive mechanism for launch/release system of payloads  
C. Marin, L. Flore, I. Ciocan ..... 12

GAS TURBINE ENGINES :

♦ Traverse gear system for measuring probes angular positioning into the BRASTA wind tunnel  
V. Vilag, G. Paniagua, I. Vladuca, D. Sanchez, C. Suciuc ..... 19

♦ Short communication on additive manufacturing technology used for axial gas turbine rotor blade  
V. Vilag, C. Dobromirescu, A. Hank, C. Suciuc, R. Nicoara, M. Vladut, T. Frigioescu, A. Paraschiv ..... 27

GAS TURBINE ENGINES AND INDUSTRIAL APPLICATIONS :

♦ Experimental investigation of axial power turbine in turboshaft application  
A. Hank, V. Vilag, R. M. Catana, G. Dediu, M. C. Tarabic, C. P. Suciuc, C. Dobromirescu ..... 35

# Editorial

## Poetica Geografiei Citadine

Întreaga activitate socială este dominată astăzi de imagini ce servesc doar propriilor scopuri. De la arhitectură la amenajarea orașelor, de la artă la știință, de la viața de zi cu zi la pasiunile umane și dorințe, peste realitate se suprapun imagini. În acest proces, imaginile ajung să fie percepute ca reale, iar realitatea ajunge să se transforme în imagini.

Am ajuns într-un punct al internaționalizării nu doar geografice a imaginii, ca rezultat al generalizării și uniformizării prin abundența mijloacelor de comunicare în masa ci și ca rezultat al experiențelor de călătorie. Punctele între distanțe s-au fluidizat și au devenit coincidențe posibile de limbaj în afara timpului și spațiului.

Popasul în arhipelagurile clasice ale timpului, muzee, catedrale, palate, poate anihila însă pasivitatea observatorului deprins cu a avea și poate elibera orgoliul prin bucuria neposesivității, prin trăirea experienței raționale și emoționale ca martor al spectacolului vieții cu nenumăratele ei fețe.

În timp, experimentele revoluționare au căutat să rupă identificarea psihologică a privitorului cu imaginea servită, astfel încât să-i provoace capacitățile de a-și revoluționa propria viață, contribuind astfel la schimbarea profundă a societății.

Mai 1968, Paris: într-o societate patriarhală ce impunea modele de comportament, bazate evident și pe imagini, tinerii își doreau o mai mare libertate. Prin revolta începută în Universitatea Nanterre, parțial ca protest împotriva războiului din Vietnam și extinsă în prima universitate a Franței, Sorbona, cu o vechime de peste șapte sute de ani, orașul a fost luat într-o vremelnică stăpânire de studenți. Muncitorii s-au alăturat revendicând salarii mai mari, condiții de muncă mai bune și sindicate mai puternice. Lui René Vignet, student participant la vremea aceea, i se părea că: „Timpul cu majuscule s-a oprit. Oamenii s-au plimbat, au visat, au învățat cum să trăiască.” Însăși țesătura orașului s-a transformat în sine (...). S-a corectat perspectiva haussmaniană a bulevardelor și a centurilor verzi redistribuite și închise circulației. Fiecare, în felul lui, și-a făcut critica urbanismului” (*Enrages and Situationists in the Occupation Movement: Paris, May, 1968 by Rene Vignet | May 1, 1993, Autonomia*).

Sondajele de astăzi relevă că revolta a fost un lucru bun: a născut scurtul moment în care totul părea cu putință!

Decembrie 1989, Timișoara: oamenii tânjeau după marea schimbare!

Decembrie 1989, București: dorința acută de schimbare înflăcărează orașul și pe locuitorii săi!

Decembrie 1989, Romania: totul părea posibil!

Dintotdeauna geografia orașelor așteaptă să fie descoperită: pecetea destinului, tradițiile sociale și culturale, vicisitudinile și legitățile istoriei, pot determina traseele cunoașterii. Michel de Certeau despre „Mersul în oraș” ca parte a cărții sale, *The Practice of Everyday Life. University of California Press, Berkeley, 1984*, ia în considerare actul de a merge în oraș. Deși element de bază al existenței orașului, nu poate fi ușor de cartografiat, neputându-se releva altceva decât locurile prin care s-a petrecut mersul pe jos, practica mersului fiind o activitate a tuturor și totuși individuală.

Lansând o paralelă cu Charlie Chaplin și bastonul acestuia, dă mersului un sens personal și creativ: la pas, omul alocă fiecărui spațiu o altă semnificație. Charlie Chaplin multiplică posibilitățile bastonului său în film, decide care „funcționează” și care provoacă râsul, bazându-se constant pe ceea ce aștepta publicul de la el. Bastonul său are propria identitate, bazată pe asocierile sale, iar jocurile cu acesta nu trebuie să perturbe secvența în care apare, nemișcând loc unei creații expresive libere. În același mod, atunci când la plimbare omul parcurge traseele selectate, se poziționează în cadrul limbii, în cadrul structurilor specifice ale orașului, ale locului de muncă, ale familiei și ale parteneriatelor.

Plimbarea de relaxare, ca și plimbarea de inițiere, funcționează în condiții istorice determinate și supuse organizării ideologice. Plimbarea în context cultural și istoric de captare a amprentelor sociale, reunește adesea componentele geografice, natură, arhitectură, artă, în raport cu interesele personale. Plimbarea poate fi și o formă de performance, dar în acest periplu nu contează doar vitrina spectacolului: întotdeauna sunt alte spectacole în afară, ce așteaptă să fie descoperite.

Ec. Elena Banea,  
Decembrie 2022

# Editorial

## Poetics of Urban Geography

---

Today, the all-social activities are dominated by images that serve only their own purposes. Whether we refer to architecture and city planning, art and science, everyday life or human passions and desires, in each case we talk about images superimposing on reality. In this process, images come to be perceived as real, and reality comes to transgress into images.

We have reached a point not only of geographical globalization of the image, because of generalization and standardization through the abundance of mass media, but also because of personal travel experiences. Bridges between distances have been significantly reduced and turned into possible coincidences of language beyond time and space.

Breaks in the classic archipelagos of time (museums, cathedrals, palaces) can annihilate the passivity of the observer who is accustomed to having and can release pride through the joy of non-possessiveness by living the rational and emotional experience as a witness of the spectacle of life with its countless reflections.

Over time, the revolutionary experiments sought to break the viewer's psychological identification with the image they offered, so far as to challenge his abilities to revolutionize his own life, thus contributing to the profound changes in society.

Paris, May 1968: in a patriarchal society that imposed models of behavior, obviously also based on images, young people wanted more freedom. Through a revolt that broke up in Nanterre University, partly as a protest against the Vietnam War, and which then extended to France's greatest university, the Sorbonne, dating over seven hundred years old, the city was taken over by the students for a short time. Workers joined them demanding higher wages, better working conditions and stronger unions. To René Vienet, one of the revolting students at that time, it seemed that: "Time with capital letters has stopped. People have walked, dreamed, learned how to live." The very fabric of the city has transformed itself (...). The Haussmanian perspective of boulevards and green belts was corrected: these were redistributed and closed to traffic. Each, in his own way, brought his criticism of town planning" (*Enrages and Situationists in the Occupation Movement, Paris, May, 1968 by Rene Vienet | May 1, 1993, Autonomedia*).

Today's polls reveal that the uprising was a good thing: it gave birth to a brief moment when everything seemed possible!

Timișoara, December 1989: people longed for the great change!

Bucharest, December 1989: the acute desire for change ignites the city and its inhabitants!

Romania, December 1989: everything seemed possible!

Urban geography has always been waiting to be discovered: the seal of destinies, social and cultural traditions, the vicissitudes and legalities of history can trace the paths of knowledge.

Michel de Certeau on "Walking in the City" as part of his book, *The Practice of Everyday Life*. University of California Press, Berkeley, 1984, speaks about the act of going downtown. Although a basic element of the city's existence, cannot be easily mapped, the only things that can be revealed are the places visited while walking along, the practice of walking being a popular activity and yet a very personal one.

Drawing a parallel with Charlie Chaplin and his cane, he gives walking a personal and creative meaning: when he steps, man assigns a different meaning to each space. Charlie Chaplin multiplies the possibilities of his cane in the film, decides which ones "work" and which stir laughter, constantly relying on what the audience expected from him. His cane has its own identity based on his associations, and his playing must not disrupt the sequence in which it appears, leaving room for free expressive creation. Similarly, when a person goes for a walk along the selected routes, he positions himself within a certain language, within the specific structures of the city, his workplace, his family and partnerships.

The relaxation walk, like the initiation walk, works under determined historical conditions and is subjected to an ideological organization. Walking in a cultural and historical context to capture social imprints often brings together geographical components, nature, architecture, art that are closely related to personal interests. Walking can also be a form of performance, but it is not only the 'shop window' of the show that matters along this journey: there are always other shows beyond it waiting to be discovered.

Ec. Elena Banea,  
December 2022

# INTELLIGENT CROSSING FOR REDUCING TRAFFIC JAMS

Remus STOICA<sup>1</sup>, Mihaela ROMAN<sup>1,2</sup>, Daniel LALE<sup>1,2</sup>

Received: 17.11.2022  
Accepted: 15.12.2022  
Published: 22.12.2022

**Copyright:** The article is an Open Access article and it is distributed under the terms and conditions Creative Commons Attribution (CC BY) license (<https://creativecommons.org/licenses/by/4.0/>).



**ABSTRACT:** One of the current struggles nowadays are dealing with traffic congestion, an increase in the number of drivers, an increase in the number of cars and an inadequate infrastructure, aspects which affect both public and individual transportation. Infrastructure options include the construction of new bridges and passageways, as well as the by-passing of roadways. The present traffic signaling system employs time-programmable automation, in which the transition duration is determined on a regular basis and is not affected by traffic flow. At the same time, traffic signal systems do not consider the instance of a car that has problems and is not able to move, or road works that further complicate the traffic conditions. This paper conducts a study regarding the proposal of utilizing inductive loop detectors for reducing traffic jams and optimizing the traffic flow.

**KEYWORDS:** Intelligent Crossing, Magnetic Field, Eddy Current, Conductive Material, Flux Density

## NOMENCLATURE

$f$  [Hz] – Operational frequency  
 $I$  [A] – Current in the coil  
PTV Vissim - Traffic in Cities: Simulation Model  
FEMM - Finite Element Method Magnetics

## 1. INTRODUCTION

The urban environment no longer allows the development and expansion of larger road lanes. In order to better manage traffic and streamline it, we can try traffic monitoring and control solutions (intelligent traffic light intersection), (video cameras in intersections with manual control of traffic lights) or by using the road space (ex. widening a street with 2 lanes), (creation of special lanes for public transport) [1].

The main goals of intelligent tutoring systems of modern traffic management are the safety of road users, improving the access in crowded urban areas and reducing congestion and accidents. In this context, several detection ways were improved and various technologies for traffic control were also ameliorated to inform (warn) the road users [2].

The basic but well-loved proximity sensor is a binary device that simply tells whether a metallic object (the “target”) is present – or not. It comprises a wire coiled around a ferromagnetic core and an oscillator to generate an alternating current to create the time-varying magnetic field [3]. When installed in different areas usually at some distance upstream junctions, this equipment can be integrated into a local data collect traffic system, in addition to their classic aim of informing the drivers [2].

The final step in the technology of traffic lights in this period was automatic timers that allowed the creation of staggered systems of signals to maximize traffic mobility. It was possible to automatically time all the traffic lights on a street, so that traffic moving in one direction and traveling at a fixed speed (usually 25 mph) would encounter only green lights. Like boulevard stops, this facilitated travel to the suburbs, but also made some provision for cross traffic and pedestrians. This system worked better on a one-way street, but even on two-way streets, lights could be set to help inbound commuters in

<sup>1</sup> Romanian Research and Development Institute for Gas Turbines COMOTI, Automation and Electrical Engineering Department.

<sup>2</sup> University Politehnica of Bucharest.

the morning, outbound in the afternoon. The engineering was complex in many ways, since traffic engineers had to estimate not just average speeds, but also acceleration and braking times [4].

## 2. SOFTWARE SIMULATION

A traffic management system can be a set of programs that provides development solutions for optimal control of traffic lights, in relation to traffic fluctuations. If an independent intersection, apply the ignition switch light signals at fixed intervals (classical automation systems), or adaptive control programs against traffic fluctuations from measurements instantly [1].

In order of obtaining accurate results, the motion of the vehicle can be calibrated in the simulator so that the control unit to resemble the local traffic conditions. The program allows total control and flexibility, so that the details of the application can be selected with ease without making compromises, avoiding costly mistakes. Executing an experiment in the real world would require high costs, the simulation representing a favorable and adequate option. By simulating with the PTV Vissim program, different simulation models can be tested by optimizing the traffic signal to test which algorithm works better. It may model and investigate any direction and kind of priority and road traffic signaling, from basic crossings to road junctions and roundabouts, as well as priority signs of public transportation and pedestrian zones or roundabouts.

The simulation was executed in the Vissim program an electrically signalized intersection with 3 roads. The intersection has one traffic light on the secondary road and two on the main road, as it can be observed in Fig. 1.

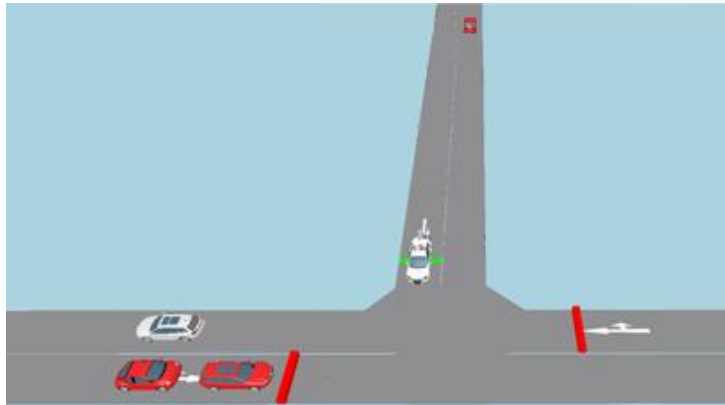


**Fig. 1. The PTV Vissim simulation of a traffic light intersection**

The example consists in streamlining the traffic of an intersection without electric traffic lights. The main road has priority, and vehicles on the secondary road must wait as in the following example in Fig. 2.

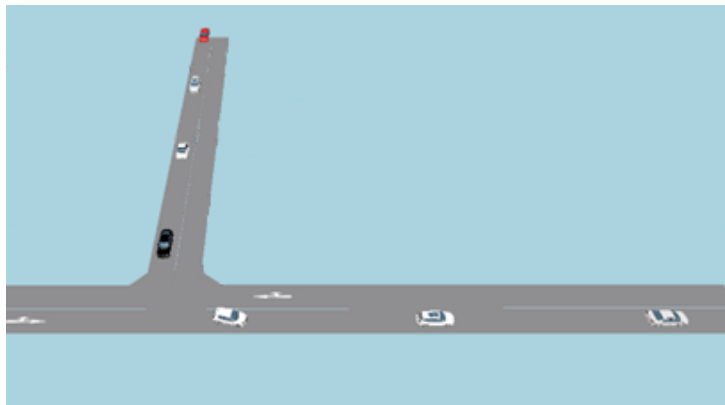


**Fig. 2. The PTV Vissim design of an intersection without traffic lights**

In case of road intersections within a section, they must operate under coordinated, considering specific programming parameters that section [1]. Fig. 3 represents the secondary road with stationary vehicles, causing agglomeration, while Fig. 4 represents the fluidization of the traffic using the intelligent crossing system of the traffic lights.

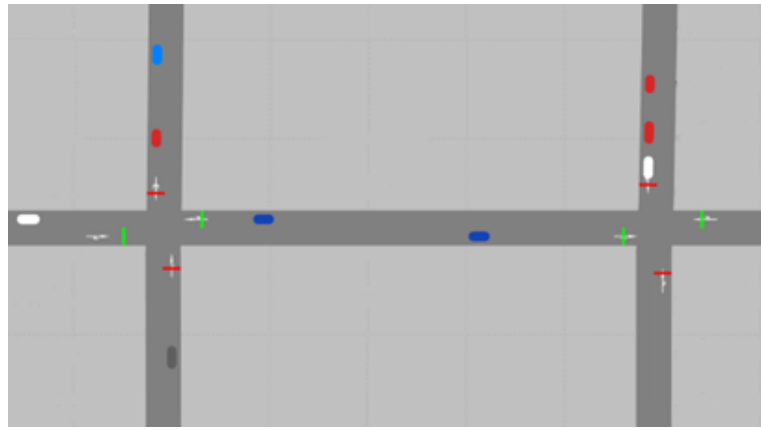


Fig. 3. The PTV Vissim simulation of the 2D traffic lighted intersections

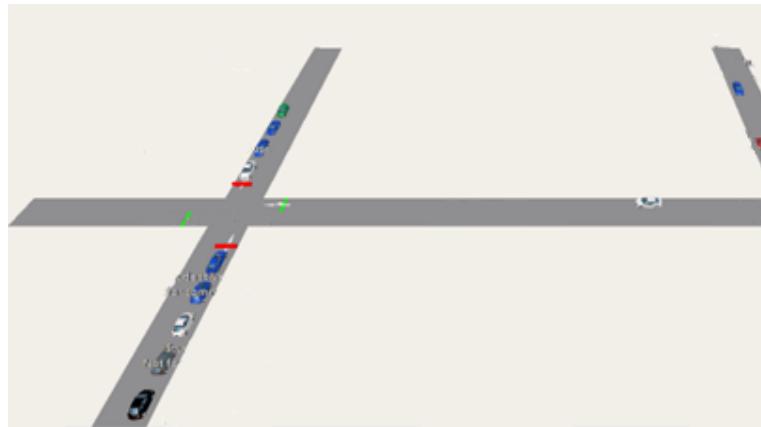


Fig. 4. The PTV Vissim simulation of 3D traffic lighted intersection

### 3. THE DETECTION SYSTEM

The intelligent crossing system includes inductive loop detectors, video imaging, laser radars, ultrasonic sensors, infrared radars, or devices that use multiple types of detectors. The information is provided to help provide the people responsible for traffic with the knowledge necessary to select the appropriate technology for the specific application. Induction loops are an electromagnetic detection system that are implemented on the road for vehicle detection. Induction loops are used for transmitting and receiving communication signals or for detecting metallic objects. An electrically isolated loop is installed in the road, applying an alternating current at frequencies between 10 kHz and 200 kHz. Inductive loop detectors have become the most common method of traffic detection since their introduction 50 years ago, this technology being a relatively recent novelty introduced for the fluidization of the traffic flow. The loop must be placed more than 5 centimeters beneath the road surface. The resistance of the wire to the flow of alternating current increases with frequency since the conducting area of the wire decreases due to the non-uniform flux inside the wire.

The loop is made up of turns made with an uninterrupted conductor that enters and exits through the same point. The two ends of the wire are connected to an extension cable as can be seen in the following figure, which in turn is connected to the detector. The detector feeds the current loop, which has a magnetic field in its area. When a vehicle or other metal object passes over the loop, the resonant frequency will increase.

The principle of operation is as follows: at the appearance of a vehicle, the inductive detector generates a pulse which "forces" the microcontroller to enter the "reading time" subroutine. This subroutine reads the instantaneous value of clock and saves it in the internal memory of the microcontroller. Then, the main program accesses these values in the internal memory of the microcontroller to calculate the speed, vehicle length and the flow [2].

Inductive detectors were selected as a result of previous analysis, but the quickly evolution of efficiency-reliability/cost ratio for some sensors (e.q. video detection), has led us to design the compatibility of controller connection, with several types of detectors [2]. The principle of operation of the detector is based on eddy currents, schematized in Fig. 6. Relying on the induction law, eddy currents are induced in a part that conducts

electric current through magnetic fields using a coil. When a vehicle passes or is stopped in the loop, because the body and the engine are made of a ferromagnetic material, there is an increase in the inductance of the coil. At the same time, the signal applied to the coil is of alternating current so that eddy currents are produced, resulting in a decrease of the inductance.

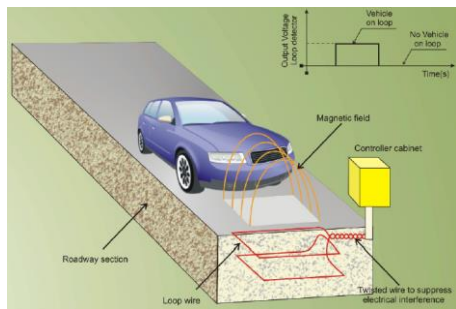


**Fig. 5. Road monitoring system using an inductive loop [2]**

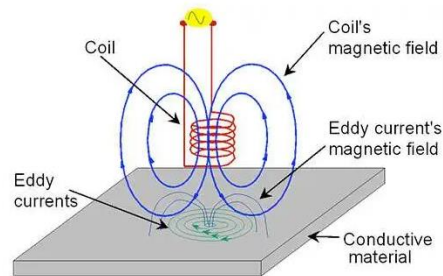


**Fig. 6. Eddy currents [3]**

The total effect is a decrease in inductance and automatically in the impedance. A relay can be connected in series with this coil, so that if the impedance of the assembly drops enough when a vehicle passes, this relay can be activated and send a traffic signal to signify the presence of the vehicle.

The detection of a vehicle is not based on its weight, but on the size of the metal surface above the loop. The figure above illustrates the magnetic flux lines. To reproduce an induction coil used in some countries since the 80s, a FEMM simulation of an induction coil installed 10 cm from the road and 2 cars that will travel a road from right to left has been executed.

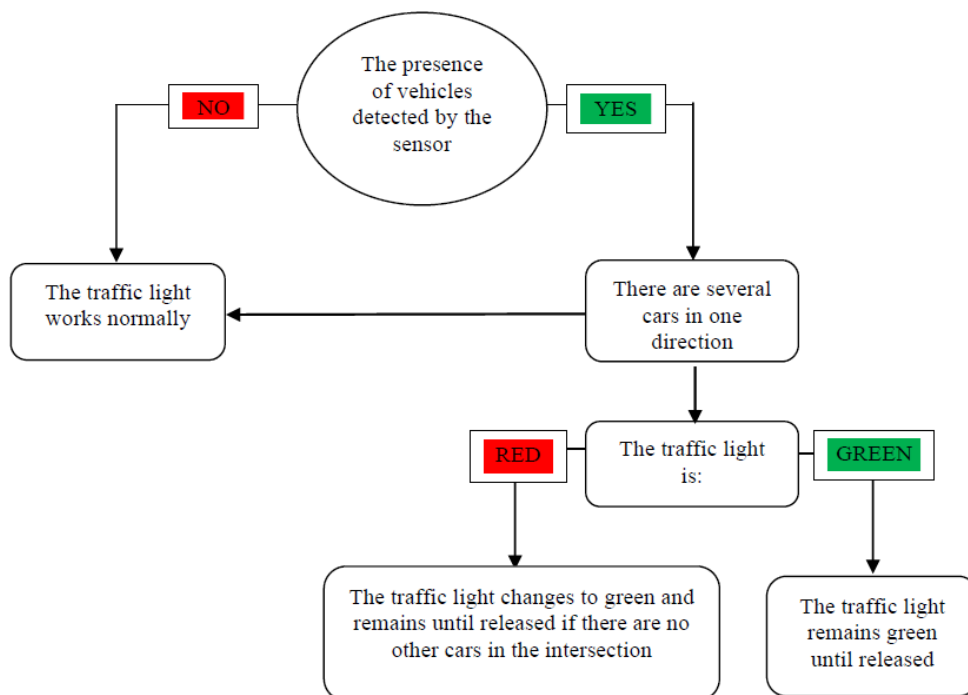


**Fig. 7. Logic diagram of the operating mode using the detection system**

Keeping in mind the simulation presented via the PVT Vissim program for the traffic density, mimicking a real-life intersection, a new simulation has been executed in order of observing the inductance dependence of the detection coil for three distinct stages: before the vehicle approaches the detection coil, the moment when the vehicle is above the detection coil and the moment after the vehicle has passed the detection coil. Those situations have been modeled and preprocessed via the FEMM program in order of displaying the coil's inductivity characteristic while a car passes through the detection system. It is worth mentioning that the detection system, at this moment, is not considering the length of the vehicle.

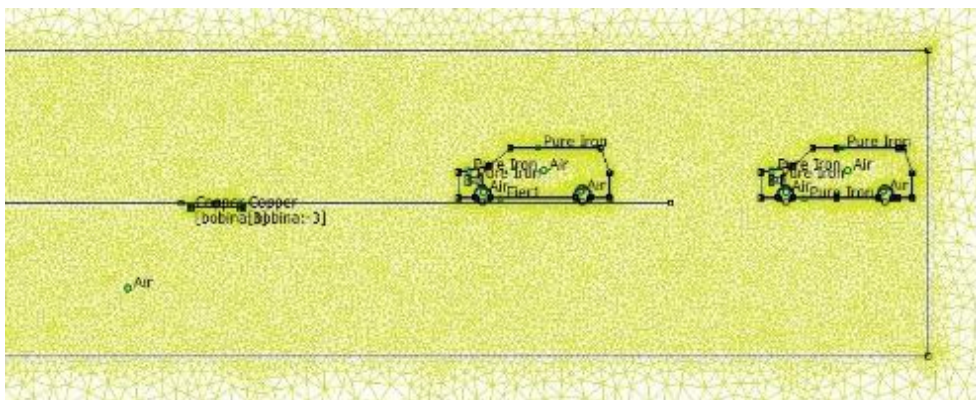


Fig. 8. The FEMM preprocessing, where the vehicles are approaching the detection system (simulation processed at  $f = 10$  kHz and  $I = 0.1$  A)

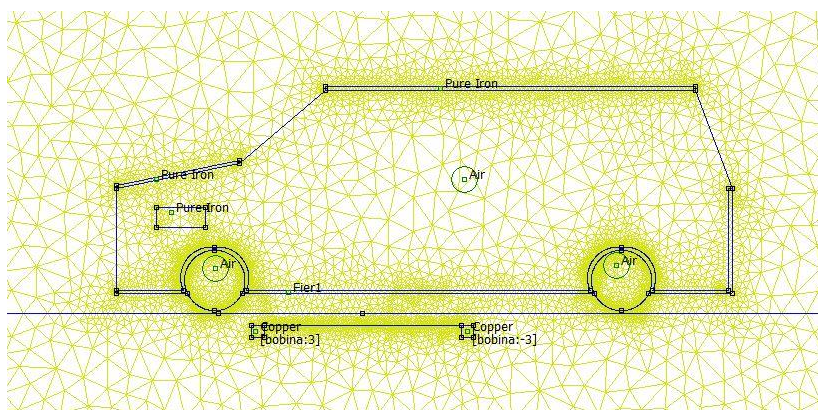


Fig. 9. The FEMM preprocessing of the vehicle above the coil installed (simulation processed at  $f = 10$  kHz and  $I = 0.1$  A)

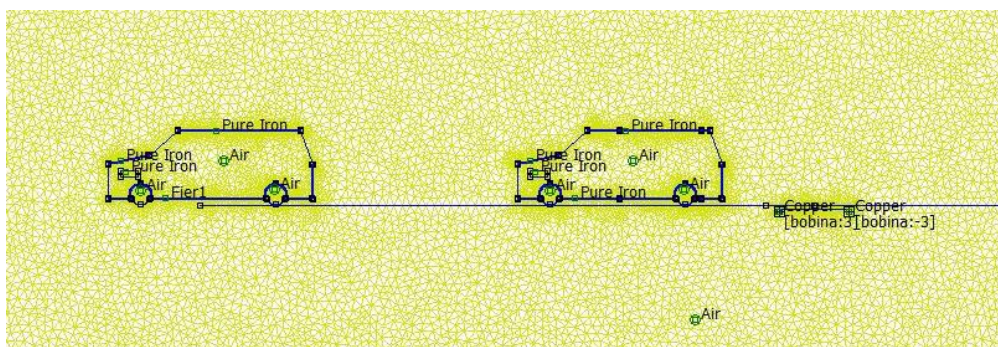


Fig. 10. The FEMM preprocessing when the cars have passed the detection coil (simulation processed at  $f = 10$  kHz and  $I = 0.5$  A)

#### 4. RESULTS

We simulated the machines moving from right to left to see how the impedance and the actual voltage at the detector terminals change by integrating them into a graph. In order the reproduction of an induction coil that is used in some countries from the 80's, we simulated, in the FEMM program, the induction coil that was installed at 10 cm from the road and 2 cars that will travel a road from right to left. It can be seen how in the 2 graphs the impedance and the effective voltage at the detector terminals decreases in the places where the car crosses over the detection sensor through eddy currents.

The following figures exemplify the three stages simulated in the FEMM program for the detection coil used for the isolated intersection control, giving us the characteristics for the inductivity and effective voltage during the process.

The first stage presents the state of the Eddy current of the detection coil before the vehicle passing.

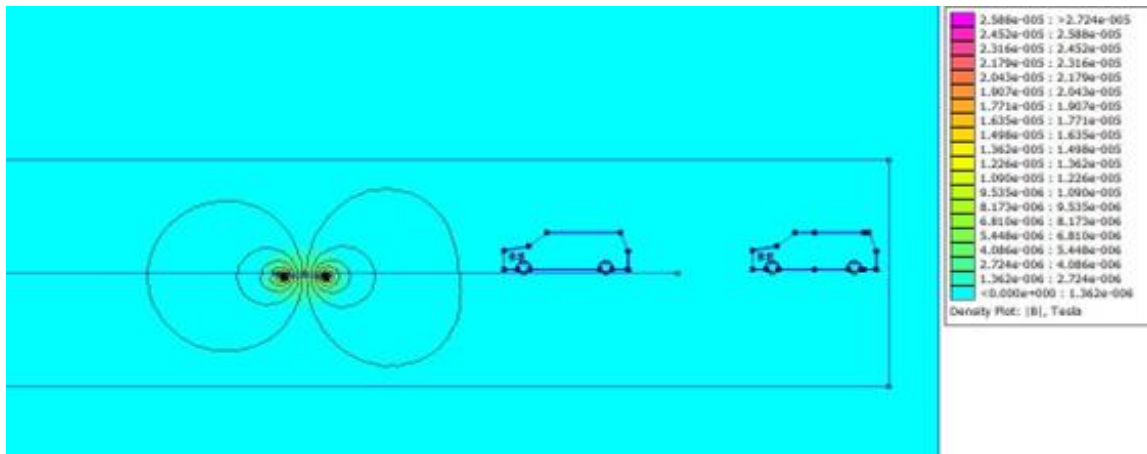


**Fig. 11. The FEMM postprocessing, where the vehicles are approaching the detection system (simulation processed at  $f = 10$  kHz and  $I = 0.1$  A)**

The second stage exemplifies the Eddy current's dependency while a vehicle is passing above the detection system.

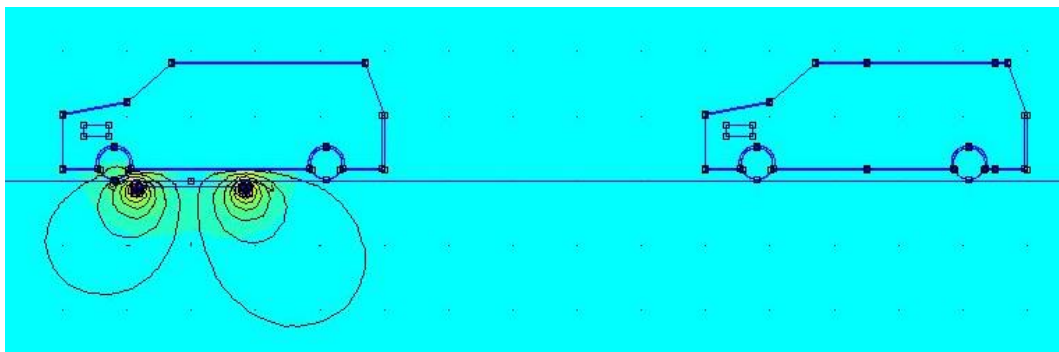


**Fig. 12. The FEMM postprocessing of the flux density when the vehicle is above the coil (simulation processed at  $f = 10$  kHz and  $I = 0.1$  A)**

The third stage is putting into perspective the effect of the vehicle successfully passing above the detection system, displaying the characteristics of the Eddy current returning to the initial state and being ready for a new detection (the simulation has been executed keeping in mind a distance between the two vehicles of 10 m).

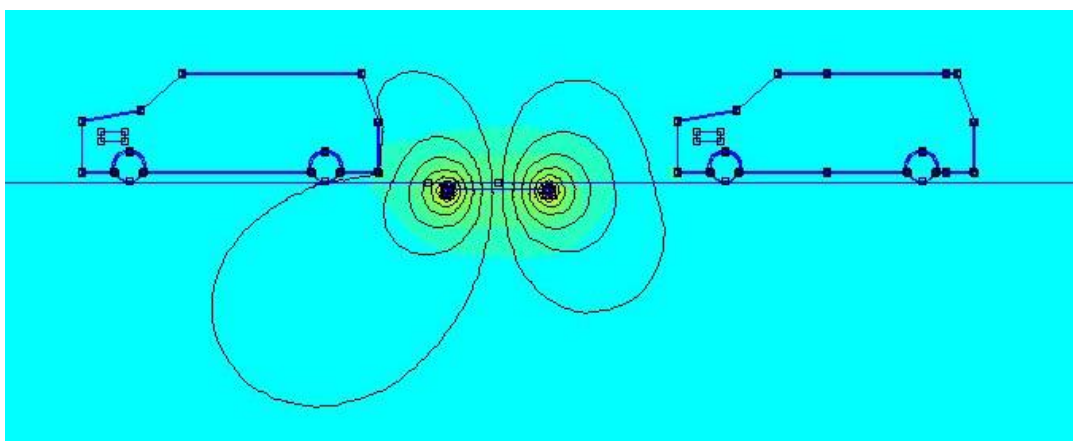


**Fig. 13. The FEMM postprocessing when the coil is placed between the passing vehicles (simulation processed  $f = 10$  kHz and  $I = 0.5$  A)**

The following tables present the characteristics of the detection coil's inductivity and effective voltage during the three stages of a vehicle passing above the detection system, on 25 meters.

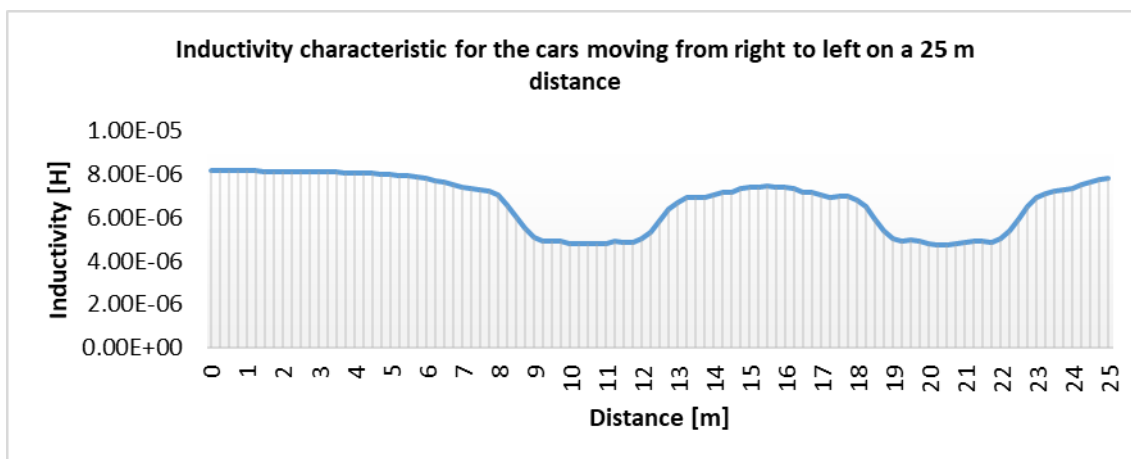


Fig. 14. Inductivity characteristic for the cars moving from right to left

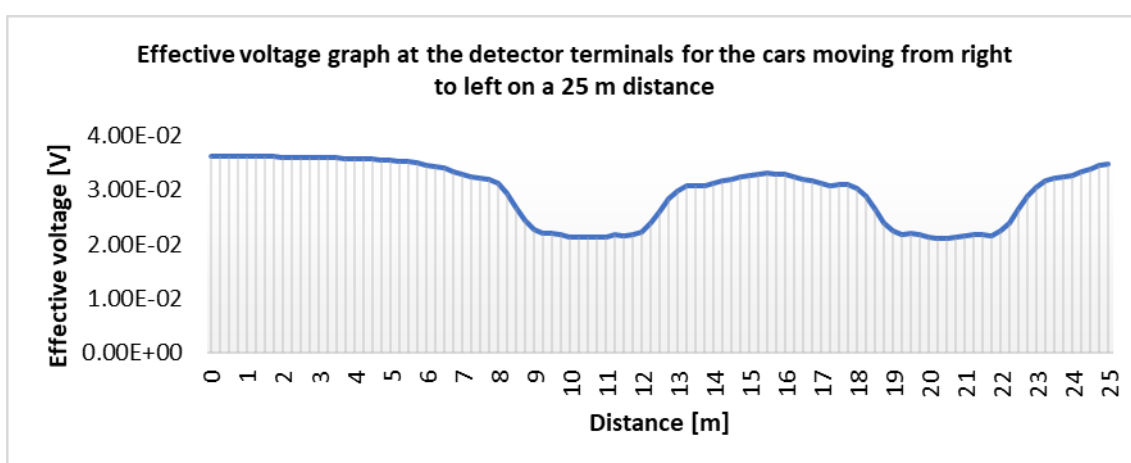


Fig. 15. Effective voltage graph at the detector terminals for the cars moving from right to left

## 5. CONCLUSIONS

The improvement of town traffic condition is largely dependent on the modern ways of traffic management and control. Advanced traffic signal controllers and control system contribute to the improvement of the traffic problem. The intelligent of traffic signal controller is introduced in this project with powerful functions and hardware interface [5].

In order of reduce pollution and to streamline traffic in big cities, traffic monitoring is one of the solutions. Cars at start-up consume more and pollute more. Therefore, if we streamline traffic, pollution will decrease, and we will gain time.

The first stage is to design a program, which consists of reading, research, planning and designing a program. Design a traffic light using the state machine is very difficult compared to design using the logic gates [5].

A 3-point traffic light intersection was simulated. Before, the intersection had a main road and a secondary road where it was congested. After the implementation of the traffic lights, the intersection became more fluid, which led to a decrease in pollution and the time spent in traffic.

An induction coil has been reproduced. From the simulation we only consider the inductive aspect of the problem, there will be capacitive effects that will change the total impedance. With the help of eddy currents, we can use this as a counter for vehicles, these being connected to a relay and an electronic module. Every time a vehicle passes, the relay is activated and the electronic module registers making the decisions to change the colors of the traffic lights.

Improvements could be made to normally running intersections. With the help of sensors that can be installed in intersections to number the vehicles and the time changes according to an algorithm. One of the problems raised by the detection system is the determination of the necessary time needed for the vehicles to pass at the green light in accordance with the size of the vehicle.

The solution for this will be illustrated in future research, where a specific algorithm will be thought out, keeping in mind the type of intersection (in our case, two intersections composed of four roads), the length of a vehicle (from a pedestrian's car to a larger scale vehicle) and the calculation of the necessary time needed for each vehicle to successfully go through the intersection.

The premises of the algorithm, at this stage, is based on calculating the time needed for a vehicle passing above the detection coil by keeping track of the inductance activity of the Eddy currents from the moment a vehicle is detected until it's passing, while also keeping track of the number of vehicles that has been registered previously, utilizing two separate detection coils, one for keeping track of the number of the cars and the other one keeping track of the cars passing through at the green light (the change of the light will be made in accordance with either a pre-established timer either dependent of the number of cars registered on the road).

## REFERENCES

- [1] Borcoși and A. Nicolae, "MODERN SYSTEM FOR MANAGEMENT OF ROAD AT AN INTERSECTION," *Analele Universității "Constantin Brâncuși" din Târgu Jiu, Seria Inginerie*, no. 2/2012, pp. 163–171, [Online]. Available: [https://www.utgjiu.ro/revista/ing/pdf/2012-2/19\\_Ilie%20BORCOSI.pdf](https://www.utgjiu.ro/revista/ing/pdf/2012-2/19_Ilie%20BORCOSI.pdf)
- [2] M. Mircea and F. Nicolae, "Increasing of the urban traffic surveillance by automatic information device," *Open Engineering*, vol. 4, no. 2, Jan. 2014, doi: 10.2478/s13531-013-0152-3.
- [3] P. Mannion, "The difference between inductive proximity, displacement, and eddy-current sensors," *EDN*, Mar. 23, 2016. <https://www.edn.com/the-difference-between-inductive-proximity-displacement-and-eddy-current-sensors/>.
- [4] C. Mcshane, "The Origins and Globalization of Traffic Control Signals," *Journal of Urban History*, vol. 25, no. 3, pp. 379–404, Mar. 1999, doi: 10.1177/009614429902500304.
- [5] S. S. Chavan, R. S. Deshpande, and J. G. Rana, "Design of Intelligent Traffic Light Controller Using Embedded System," *2009 Second International Conference on Emerging Trends in Engineering & Technology*, 2009, doi: 10.1109/icetet.2009.76.
- [6] L. Bhaskar, A. Sahai, D. Sinha, G. Varshney, and T. Jain, "Intelligent traffic light controller using inductive loops for vehicle detection," *2015 1st International Conference on Next Generation Computing Technologies (NGCT)*, Sep. 2015, doi: 10.1109/ngct.2015.7375173.
- [7] S. S. Mohammed Ali, B. George, and L. Vanajakshi, "Mutually coupled multiple inductive loop system suitable for heterogeneous traffic," *IET Intelligent Transport Systems*, vol. 8, no. 5, pp. 470–478, Aug. 2014, doi: 10.1049/iet-its.2013.0055.
- [8] W. de Queiróz Lamas, "Intelligent Urban Traffic Flow Control: A Case Study on Fuzzy Logic Application," *International Journal of Transportation Engineering and Technology*, vol. 3, no. 3, p. 25, 2017, doi: 10.11648/j.ijtet.20170303.11.
- [9] P. Mirchandani and Fei-Yue Wang, "RHODES to intelligent transportation systems," *IEEE Intelligent Systems*, vol. 20, no. 1, pp. 10–15, Jan. 2005, doi: 10.1109/mis.2005.15.
- [10] F. Mocholí Belenguer, A. M. Millana, A. Mocholí Salcedo, and V. Milián Sánchez, "Vehicle modeling for the analysis of the response of detectors based on inductive loops," *PLOS ONE*, vol. 14, no. 9, p. e0218631, Sep. 2019, doi: 10.1371/journal.pone.0218631.
- [11] H. Dong, X. Wang, C. Zhang, R. He, L. Jia, and Y. Qin, "Improved Robust Vehicle Detection and Identification Based on Single Magnetic Sensor," *IEEE Access*, vol. 6, pp. 5247–5255, 2018, doi: 10.1109/access.2018.2791446.

# PHYSICAL AND MATHEMATICAL MODEL OF THE ELECTRIC DRIVE MECHANISM FOR LAUNCH/RELEASE SYSTEMS OF PAYLOADS

Constantin MARIN<sup>1</sup>, Lica FLORE<sup>1</sup>, Ion CIOCAN<sup>1</sup>

Received: 20.07.2022

Accepted: 17.10.2022

Published: 22.12.2022

**Copyright:** The article is an Open Access article and it is distributed under the terms and conditions Creative Commons Attribution (CC BY) license (<https://creativecommons.org/licenses/by/4.0/>).



**ABSTRACT:** Implementation and development of electromechanical actuator (EMA) has rapidly increased during the last years in the context of the “more electrical aircraft”. The main technical problem for the implementation of EMA is the jamming. This phenomenon can appear due to metal-metal contact of load transmission. This problem penalizes the reliability although with very low failure rate. Several ways to overcome this problem in aeronautical EMAs are currently being investigated and one of the most attractive and promising way in solving this problem consists in choosing the advanced materials and friction control. One of the objectives of the study carried out for the development of a carriage and release payloads mechanism (EAL) for aircraft consisted in establishing the design requirements of the linear electromechanical actuator in accordance with the imposed performances. To achieve this objective, the force required for the EAL’s unlocking action and the geometry of the compression spring of the actuator were defined and the elastic characteristics of this part were determined. To optimize the geometry and the elastic characteristic of the spring, a mathematical modeling program based on the functions, equations and inequalities that define the compression helical spring has been drawn up.

**KEYWORDS:** Actuator, Release, Ejection, Rack, Spring

## NOMENCLATURE

EAL	Carriage and release payloads mechanism (Ejector rack)
EMA	Electromechanical Actuator
LEMA	Linear Electromechanical Actuator
$D$	spring wire diameter
$D_m$	mean coil diameter
$G$	modulus of rigidity for the spring material
$d$	wire diameter
$t$	pitch of spring
$n$	number of active turns
$H_1$	preloaded spring length
$H_{max}$	spring length at $F_{max}$
$H_0$	spring free length
$H_b$	spring length at $F_b$
$\delta_b$	spring deformation at $F_b$
$\delta_1$	spring deformation at $F_1$
$F_{max}$	maximum force
$i$	ratio between mean coil diameter and coil wire diameter

<sup>1</sup> Romanian Research and Development Institute for Gas Turbines COMOTI, Bucharest, Romania

$\alpha_0$	coil angle
$J$	coil gap
$K_i$	linear helical spring slope
$F_l$	preloaded force
$\delta_{max}$	maximum spring deformation
$F_a$	unlocking force
$F_b$	locking force

## 1. INTRODUCTION

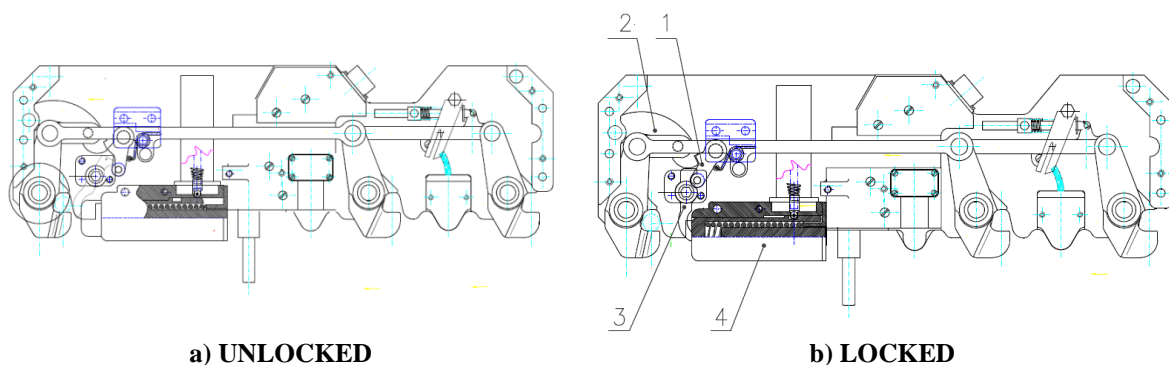
Competitiveness in high-end industrial fields such as aerospace constructions has led to an increasing demand for high performance equipment made by unconventional and non-polluting technologies. These should be adapted to maximize performance associated with low consumption of energy and with as little impact on the environment as possible. Thus appeared the concept of "more electric, concept embraced today by all researchers in the field of aeronautics [1]. A reasonable use of energy in all its aspects along with the reduction of pollution are conditions without which nowadays' sustainable development of humanity seems unconceivable. In this regard, together with the classical pyrotechnical actuators, other less known and used electrical actuators are more and more subjected to studies. These "unconventional" mechanisms usually have several advantages that qualify them for niche utilizations [2]. Such a technical solution is the carriage and release payloads mechanism for aircrafts.

The areas of use for actuators in aircraft are highly diverse and in accordance, the actuators must meet different requirements. The most important requirements on the aircraft actuators are: an optimal volume/performance ratio, low power consumption, temperature resistance, long life of usage, resistance against vibrations and impact and high corrosion resistance.

Actuators convert electrical signals to mechanical movement or other physical variables, such as pressure or temperature and thus play an active role in control systems. For some fields of application, such as aviation, it is important that the actuators achieve very high dynamic forces but also be lightweight and able to be fitted into small and tight spaces. They also must withstand ambient conditions such as strong vibrations and heat and cold fluctuations.

The electromagnetic actuators are used in most aircraft systems. For example, these devices can be found in water, oxygen, hydraulic, fuel and air systems. Furthermore, the electromagnetic actuators that are equipped with valves fulfill safety functions by interrupting the flow in case of an emergency.

The carriage and release payloads mechanism (EAL) developed in COMOTI, figure 1, was intended for taking over and transporting the payloads safely during the captive flight and the ordered launching. In this paper the aspects and requirements imposed by the correct operation of the unlocking control subassembly will be analyzed.



a) UNLOCKED

b) LOCKED

Fig.1. Carriage and release payloads mechanism (EAL)

1- Locking lever, 2 - Curved lever, 3 - Actuating lever, 4 - Linear Electromechanical Actuator (LEMA)

Linear electromechanical actuators are used frequently in the equipment of weapons systems, installed on military aircraft of Western origin. The hooking and launching equipment with electric operation vs. pyrotechnic operation have a series of advantages such as decreasing loads of the components, increasing the reliability of the equipment and diminishing the risk of malfunction and an easier maintenance.

The American company MOOG is a pioneer in the design and manufacture of linear electromechanical drives for weaponry equipment [3]. A piston driven by a precompressed spring whose operating control is provided by a rotating solenoid provides the useful force.

When this solenoid is activated by an electrical control signal it moves a plunger in a perpendicular plane to the direction of linear motion of the piston for locking and unlocking of the payloads. Due to a unique design, the operation of the linear electromechanical actuator (LEMA) can only be activated by an electrical impulse and is insensitive to shock and/or uncontrolled activation. Thus, the patented constructive solution offers many forces (up to 56.6 daN) in a device of relatively small dimensions, its operation being almost instantaneous and with a high degree of safety. The actuators produced by the MOOG Company can be found in most of the ejector rack units (BRU- Bomb Release Unit) that equip the aircrafts [4].

## 2. UNLOCKING FORCE CALCULATION

According to the figure 1, in order to unlock the carriage and release payloads mechanism (EAL) it is necessary for the force ( $F_a$ ), see figure 2, of the linear electromechanical actuator (4) to develop a torque applied to the locking lever (1) through the actuating lever (3) capable of overcoming the torque of friction force between the curved lever (2) and locking lever (1).

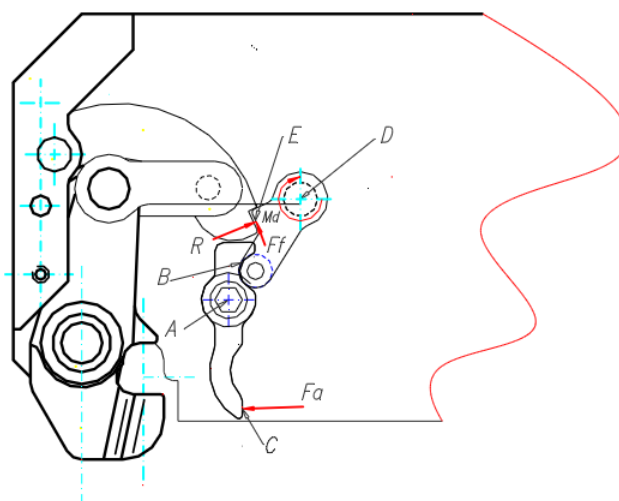


Fig.2. Detailed geometry of locking/unlocking parts

According to the figure 2, the relation (1) gives the rotation torque related to the point A:

$$M_a = F_a \times L_{AC} \quad (1)$$

The rotation of the actuating lever around its axis (point A) develops, at the point of contact of this lever with the locking lever (point B), a force  $F_b$  given by the relation: (2).

$$F_b = \frac{M_a}{L_{AB}} = \frac{F_a \times L_{AC}}{L_{AB}} \quad (2)$$

In order to remove the locking lever from contact with the curved lever (disengagement of the equipment), the moment developed by this force in the axis of rotation of the locking lever (point D), must overcome the torque of friction force between these two parts and the torque  $M_d$  locking lever spring:

$$\frac{F_a \times L_{AC}}{L_{AB}} \times L_{BD} \geq (F_f \times L_{DE}) + M_d \quad (3)$$

The friction force can be calculated with the relation:

$$F_f = \mu \times R \quad (4)$$

Where:  $\mu$  – friction coefficient and  $R$  – reaction force between curved lever and locking lever. The mathematical relation that allows the calculation of the necessary force of unlocking will be:



Where:

G = modulus of rigidity;  
 D<sub>m</sub> = mean winding diameter;  
 δ = spring deformation;  
 L=loaded length

n = number of active coils.  
 d = coil wire diameter;  
 L<sub>0</sub>=free length

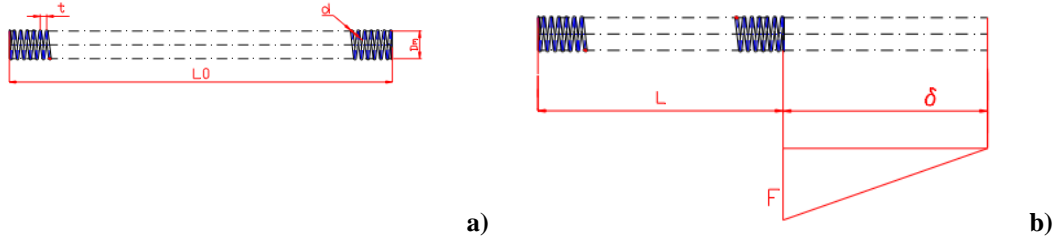


Fig.4 Compression spring: a) spring geometry, b) compressed spring geometry

From the analysis of the formulas which allowed the calculation of the elements that define the geometry and the elastic characteristic of the compression helical spring, the following conclusions could be deduced:

1. The useful force of the spring is directly proportional to the diameter of the coil wire (d) and the useful stroke (δ<sub>max</sub>) and inversely proportional to the average-winding diameter (D<sub>m</sub>) and the number of useful coils (n). The useful stroke is influenced by the free length of the spring.
2. The diameter of the coil, the average diameter of the winding influences the requirements related to the design and execution of the spring.

The optimization of the geometry and the characteristics of the spring have imposed an iterative computation performed on the computer. This has been based on a mathematical model with functions, equations and inequalities that define the helical compression spring. The basis of this calculation program was the logic diagram presented in figure 5. To reduce the number of iterations an analysis was made to estimate the range of variation of the input parameters.

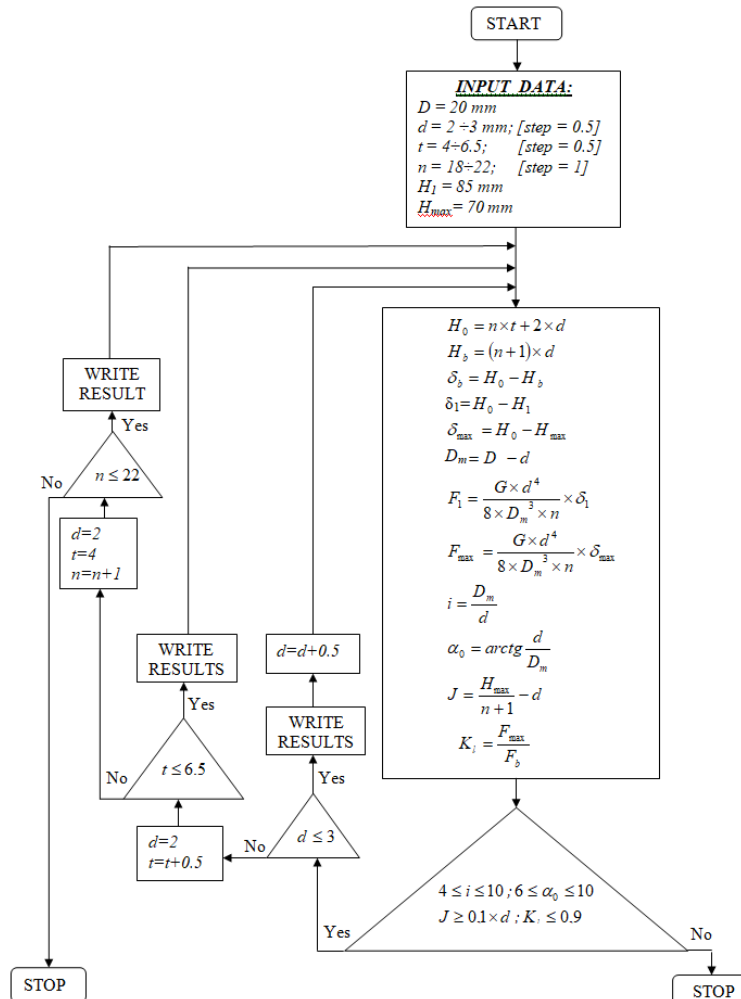
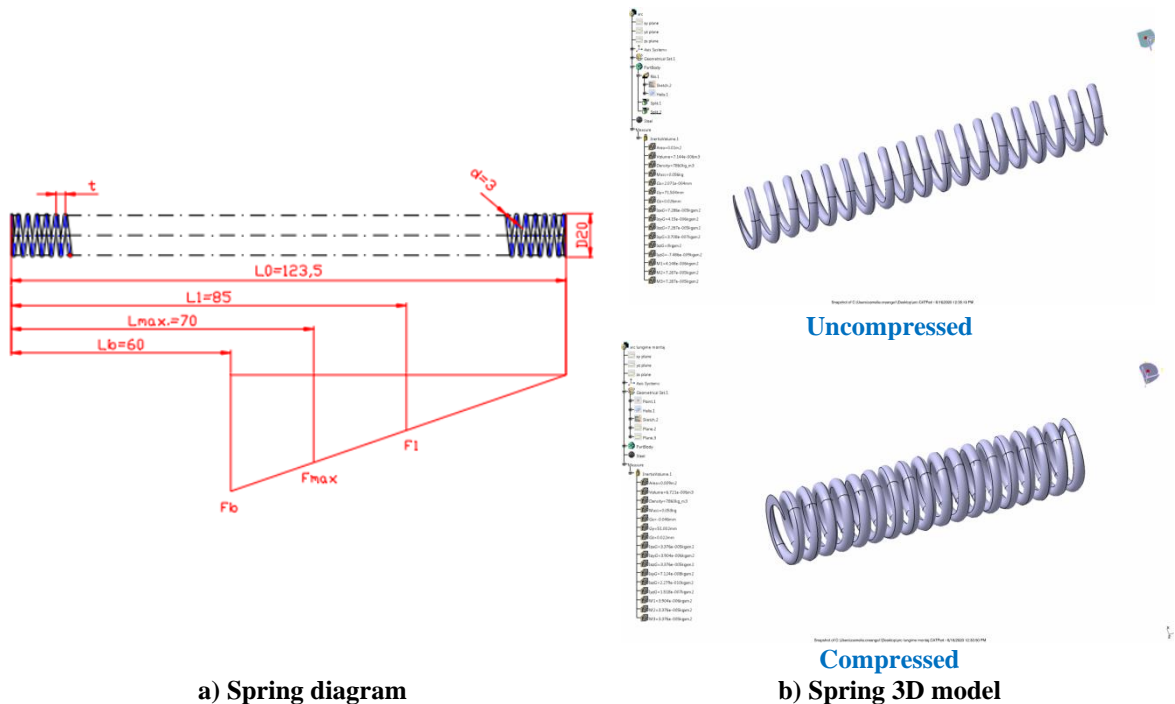


Fig. 5. Spring calculation diagram

Based on the analysis of the results (Table 1), the geometry of the compression helical spring was defined (Fig.6).

**Table 1. The results of iterations for the spring geometry calculation**

Parameter	Units	Iterations								
		1	2	3	4	5	6	7	8	9
t	mm	6,5	6,5	6,5	6,5	6,5	6,5	6,5	6,5	6,5
n	-	18,0	18,0	18,0	19,0	19,0	19,0	20,0	20,0	20,0
d	mm	2,0	2,5	3,0	2,0	2,5	3,0	2,0	2,5	3,0
Dm	mm	17,0	17,0	17,0	17,0	17,0	17,0	17,0	17,0	17,0
Lp	mm	96,0	96,0	96,0	96,0	96,0	96,0	96,0	96,0	96,0
Cp	mm	15,0	15,0	15,0	15,0	15,0	15,0	15,0	15,0	15,0
Ho	mm	117,0	117,0	117,0	123,5	123,5	123,5	130,0	130,0	130,0
H1	mm	85,0	85,0	85,0	85,0	85,0	85,0	85,0	85,0	85,0
Hmax	mm	70,0	70,0	70,0	70,0	70,0	70,0	70,0	70,0	70,0
G	daN/mm <sup>2</sup>	8000,0	8000,0	8000,0	8000,0	8000,0	8000,0	8000,0	8000,0	8000,0
Hb	mm	38,0	47,5	57,0	40,0	50,0	60,0	42,0	52,5	63,0
δb	mm	79,0	69,5	60,0	83,5	73,5	63,5	88,0	77,5	67,0
δ1	mm	32,0	32,0	32,0	38,5	38,5	38,5	45,0	45,0	45,0
δmax	mm	47,0	47,0	47,0	53,5	53,5	53,5	60,0	60,0	60,0
F1	daN	5,8	14,1	29,3	6,6	16,1	33,4	7,3	17,9	37,1
Fmax	daN	8,5	20,8	43,0	9,2	22,4	46,4	9,8	23,9	49,5
Fb	daN	14,3	30,7	55,0	14,3	30,8	55,1	14,3	30,8	55,2
i=Dm/d	-	8,5	6,8	5,7	8,5	6,8	5,7	8,5	6,8	5,7
J=Lu/(n+1)·d	mm	1,7	1,2	0,7	1,5	1,0	0,5	1,3	0,8	0,3
Kl=Fu/Fb	-	0,6	0,7	0,8	0,6	0,7	0,8	0,7	0,8	0,9
α0=arctg(d/Dm)	grade	6,7	8,36	10	6,7	8,36	10	6,7	8,36	10



**Fig.6. Defined electromechanical actuator spring and 3D model of electromechanical actuator spring**

### 5. CONCLUSIONS

In the present paper, the emphasis was on defining the constructive solution of the linear electromechanical actuator and, in correlation with the destination of this subassembly of EAL, the aim was to establish the design requirements regarding the performances imposed on this mechanism. To achieve the pursued objective, the specific aspects of the linear electromechanical actuator were approached, as follows:

- The necessary force for the unlocking of the EAL was determined by calculation. The value of this force is essential in the design of the linear electromechanical actuator;
- The geometry of the compression spring of the actuator was defined and the elastic characteristics of this part were determined;
- For the optimization of the geometry and the elastic characteristic of the spring, a mathematical modeling program was drawn up, based on the functions, equations and inequalities that define the compression helical spring;

To ensure a safe unlocking action of the equipment, at the maximum load case that has been considered, it is necessary to ensure a coefficient of friction as low as possible. Constructively, this requirement can be met by plating with a tablet of a low coefficient of friction (brass, bronze, duramide, teflon) for one of the levers surfaces.

The hooking and launching equipment with electric operation vs. pyrotechnic operation have a series of advantages: decreasing loads of the components, increasing the reliability of the equipment, diminishing the risk of malfunctions and an easier maintenance.

Currently, the electromechanical linear actuator is under testing and after the tests will be concluded and the results analyzed, it will be integrated within the carriage and release payloads mechanism (EAL). This assembly will also undergo a series of tests with the intended purpose of verifying the compatibility with the aircraft systems.

### **ACKNOWLEDGEMENT**

This work was carried out within “Nucleu” Program TURBOPROP supported by the Romanian Minister of Research and Innovation, project number PN 19.05.01.06.

### **REFERENCES**

- [1] David Koyama, How the More Electric Aircraft is influencing a More Electric Engine and More, Electrical Technologies for Aviation of the Future, Tokyo, 26-27 March, 2015;
- [2] Physico-mathematical models of the Vuilleumier machine, TERMOTEHNICA nr.2/2009;
- [3] MOOG solenoid product guide  
<https://www.moog.com/content/dam/moog/literature/MCG/solenoidprodguide2.pdf>;
- [4] Suspension, arming, and releasing equipment, CNATT Rate Training Manager, 230 Chevalier Field Avenue Pensacola, FL 32508;
- [5] PN 19.05.01.06 – B58, The physical, mathematical and numerical model of the specific mechanism to the electrical actuation of the propulsion systems and the controlled launch/release of the payloads, Comoti, July 2022.

# TRAVERSE GEAR SYSTEM FOR MEASURING PROBES ANGULAR POSITIONING INTO THE BRASTA WIND TUNNEL

Valeriu VILAG<sup>1</sup>, Guillermo PANIAGUA<sup>2</sup>, Iulian VLĂDUCĂ<sup>1</sup>, Diego SANCHEZ<sup>2</sup>,  
Cosmin SUCIU<sup>1</sup>

Received: 25.11.2022

Accepted: 19.12.2022

Published: 22.12.2022

**Copyright:** The article is an Open Access article and it is distributed under the terms and conditions Creative Commons Attribution (CC BY) license (<https://creativecommons.org/licenses/by/4.0/>).



**ABSTRACT:** The paper presents the concept, design, manufacturing, and functional tests results of a traverse gear system for angular positioning of probes into the BRASTA wind tunnel of the Purdue Experimental Turbine Aerothermal Laboratory (PETAL) at Purdue University. Starting from a preliminary design coming from the experimental needs, a final design was agreed conducting to assembly and manufacturing drawings using CAD software. A control software was developed using LabView platform to control the movement and angular position of the probes. Functional tests have been performed with the entire assembly giving satisfactory results in terms of leakage at pressures between -0.95 and 6 bars. A description of the experimental methods that will be implemented is given within the scope of PETAL facilities

**KEYWORDS:** traverse gear, wind tunnel, concept, control software, functional tests

## 1. INTRODUCTION

Scientific experiments in wind tunnels, and not only, require proper instrumentation in order to get valuable data to be used by the researchers. Apart from the obvious needed accuracy for measuring the flow parameter, such as total pressure, total temperature etc., the positioning of the probe acquiring the physical signal is also important. More, many times the spatial field of the respective parameter is required since only punctual knowledge is not enough to determine performances or other aspects related to the flow. Thus, there exist at least two options: first, using a high number of probes mounted in different positions, carefully chosen inside the spatial field, in order to build a matrix of data which describes the variation of the measured parameter in the section of interest; second, using a smaller number of probes mounted on a mobile assembly which can scan the section of interest with a certain speed (dependent on the acquisition frequency) in order to produce the same aforementioned data matrix. The latter option produces a more accurate description of the field of interest because of the flexibility given to the physical position of the probes, furthermore the major contribution comes from the side of a single calibration and manufacturing of probes that are often built of-the-shelf. Amend J & T. Povey [1] have described in their article the design and commissioning of an ultra-compact traverse system for the ECAT facility at the University of Oxford. The system was designed for a pressure of 10bar and has been tested with Kiel probes and thermocouples in a series of semi-transient 60s runs.

The current paper shows and details such a traverse system from concept to functional tests performed with the entire assembly. Specifically, the traverse system is needed to conduct experiments into the Big Rig for Aerothermal Stationary Turbine Analysis (BRASTA) [2] wind tunnel, the preliminary concept and requirements being drawn by the staff of Purdue University, Figure 1. Surveys of stagnation pressure distribution inside wind tunnels are necessary and directly dependent of the data acquisition system [3]. The recorded data can ultimately form a matrix of variables that describe de pressure field generated inside the

<sup>1</sup>Romanian Research and Development Institute for Gas Turbines COMOTI

<sup>2</sup>Purdue University, United States of America

measuring section of a wind tunnel. The size of the matrix is determined by the acquisition frequency, the probe's physical location and the length of the path from the tip of the probe to the transducer. For stagnation pressure measurement the pressure wave travels with a speed equal to the speed of sound of the surrounding medium, thus limiting a high frequency pressure reading. The traverse gear system presented in this article can provide a stable speed of movement of the probe at a certain predetermined radius in order to scan the stagnation pressure over a 30° angle inside BRASTA wind tunnel with minimum leakage, providing a suitable tool for conducting research experiments.

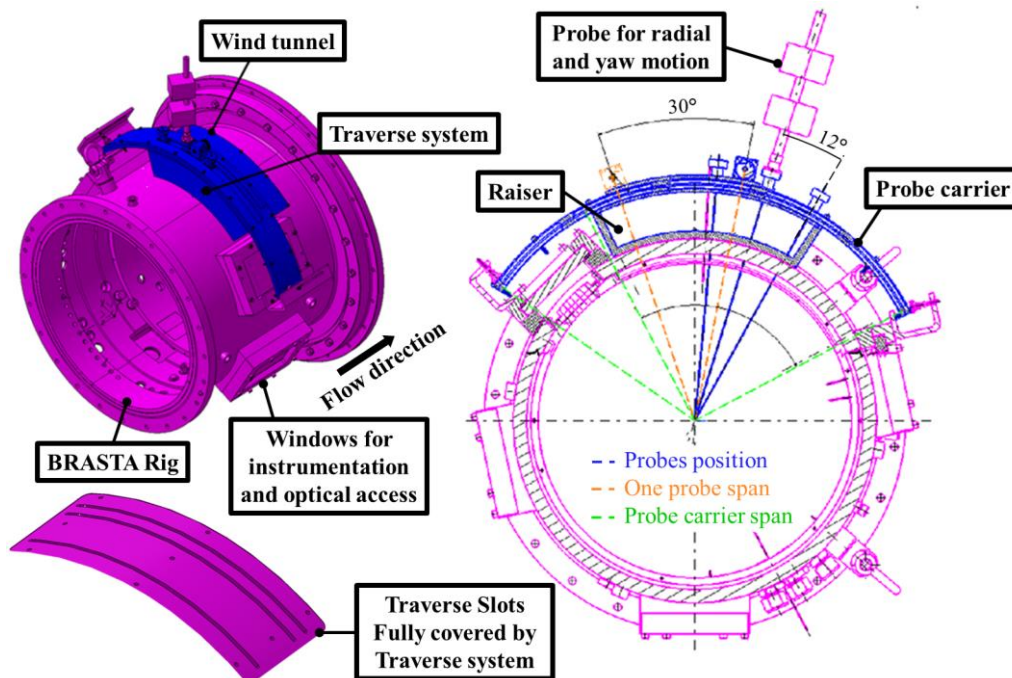


Fig. 1 Preliminary concept of the traverse system

## 2. DESIGN OF THE ASSEMBLY

The traverse gear system, Figure 2, will be mounted on a sector of BRASTA, inside which air flows at subsonic, transonic, and supersonic speeds. The rig contains three traverse slots to access the inside, at three different axial locations (separated 100 mm and 30 mm approximately), but same circumferential positions. Once BRASTA is mounted inside the wind tunnel, the traverse system will be mounted in vertical position and is designed to integrate 3 pressure probes through one of the slots at once. Therefore, the assembly must be mounted to align the probes with a particular slot. The probes are positioned at a 12° angle one from another. The probes will be mounted on the so-called probe carrier, which will move over a fixed support bracket equipped with a gear rack. The movement will be made with the help of a pinion driven by an electrical motor fixed on the mobile component. The total angle of the slots is 55.5°. The maximum angle achieved by the movement of each probe is 30°±0.2° as it can be seen in Figures 1 and 3. Hence, the traverse system provides a trade-off between circumferential span and repeatability that needs to be considered by the engineer based on the objectives of each test campaign.

The working conditions are presented in the following table:

Table 1. Working condition for BRASTA wind tunnel equipped with the traverse gear system

Parameter	Inside the tunnel	Outside the tunnel
Pressure:	1 mbarA – 7 barA	Atmospheric
Temperature:	max 500 K	293 K

The assembly has been produced from 304L stainless steel material. To be able to test the assembly, a mock-up of the BRASTA tunnel has been made from regular steel. The assembly is made from three main components: Bottom rail, Probe Carrier and Raiser (see Figure 2).

The Bottom Rail contains the gear rack used to move the Probe Carrier. The Probe Carrier holds the pressure probes supports and the movement assembly composed of: pinion, planetary reduction gear box, stepper motor and absolute position encoder. Because of the limitations imposed by the BRASTA wind tunnel, the Raiser has been designed to raise the assembly over a certain height for avoiding the obstacles created by the openings of the wind tunnel used for visual characterization of the flow such as Schlieren and PIV.

To provide static and dynamic sealing of the assembly, X-rings have been implemented because of their advantage over the O-rings (2 sealing surfaces over one side instead of just 1). X-ring's slots have been designed for Quad-Rings®/ X-Rings with a section of 5.33mm (0.21"). The X-rings allow for translation movement across them without twisting the gasket. The material used for the X-rings has been VMQ (Silicone) which is able to withstand temperatures of around 500K.

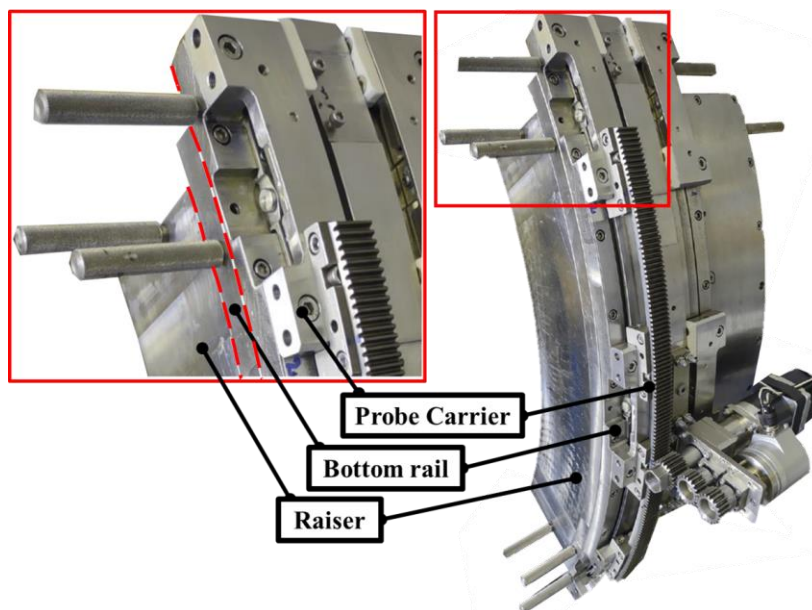


Fig. 2 Traverse Gear System components.

The stepper motor and reduction gearbox have been chosen to be able to produce a torque higher than the friction created between the X-rings and Probe Carrier. The reduction gearbox has also the role to reduce the necessary dimensions of the motor and the resonance frequencies. Figure 3 presents the final minimal and maximal angular position of the traverse gear system.

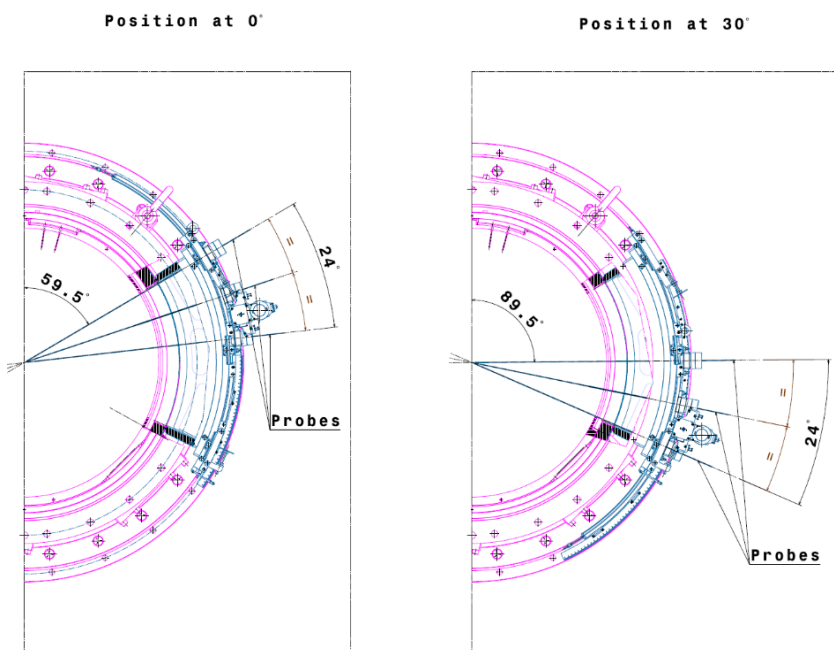


Fig. 3 Traverse Gear System Min-Max Position

The Probe Carrier is placed on a total of 12 support rollers. 6 of them are mounted directly on the bottom rail assembly while the other six are mounted on some components which provide the external support of the Probe Carrier. The rollers have been designed in order to resist to the high stresses which appear while the assembly is working under pressure or vacuum conditions.

The chosen Stepper Motor is ST 6018Lx3008B -NEMA 24 from Nanotec [4]. The torque curves of the motor point a minimum of 1Nm up to 600rpm. The reduction gearbox (GPLE60-2S-40) is acquired also from Nanotec and has a reduction ratio of 1:40 [5]. The maximum moment is 64Nm and the backlash is 12' (arc minutes). The stepper motor is an open-loop type which does not provide position feedback. In order to improve the precision in case of slippage between couplings or other possible errors, an absolute position encoder has been fitted on the mobile assembly. The encoder is from SICK (ACM60B-S1KE13x06) [6] and has a maximum resolution of 10485 steps per revolution (2' arc minutes).

The Traverse Gear System has been initially tested at COMOTI facility on the BRASTA mock-up and the leakages have been quantified. The results are presented in Table 1.

**Table 2** Leakage tests for Traverse Gear System Assembly

Test no.	Pressure [bar]	Mass flow rate [kg/s]	Pressure change domain [bar]	Average pressure change [bar/min]
1	-0.95	<0.00001	-0.9 → -0.8	0.0052
2	4	<0.00129	6 → 5	0.1
3	6	<0.00215		

After delivery, the Traverse Gear System Assembly was mounted on the BRASTA tunnel, Figure 4.

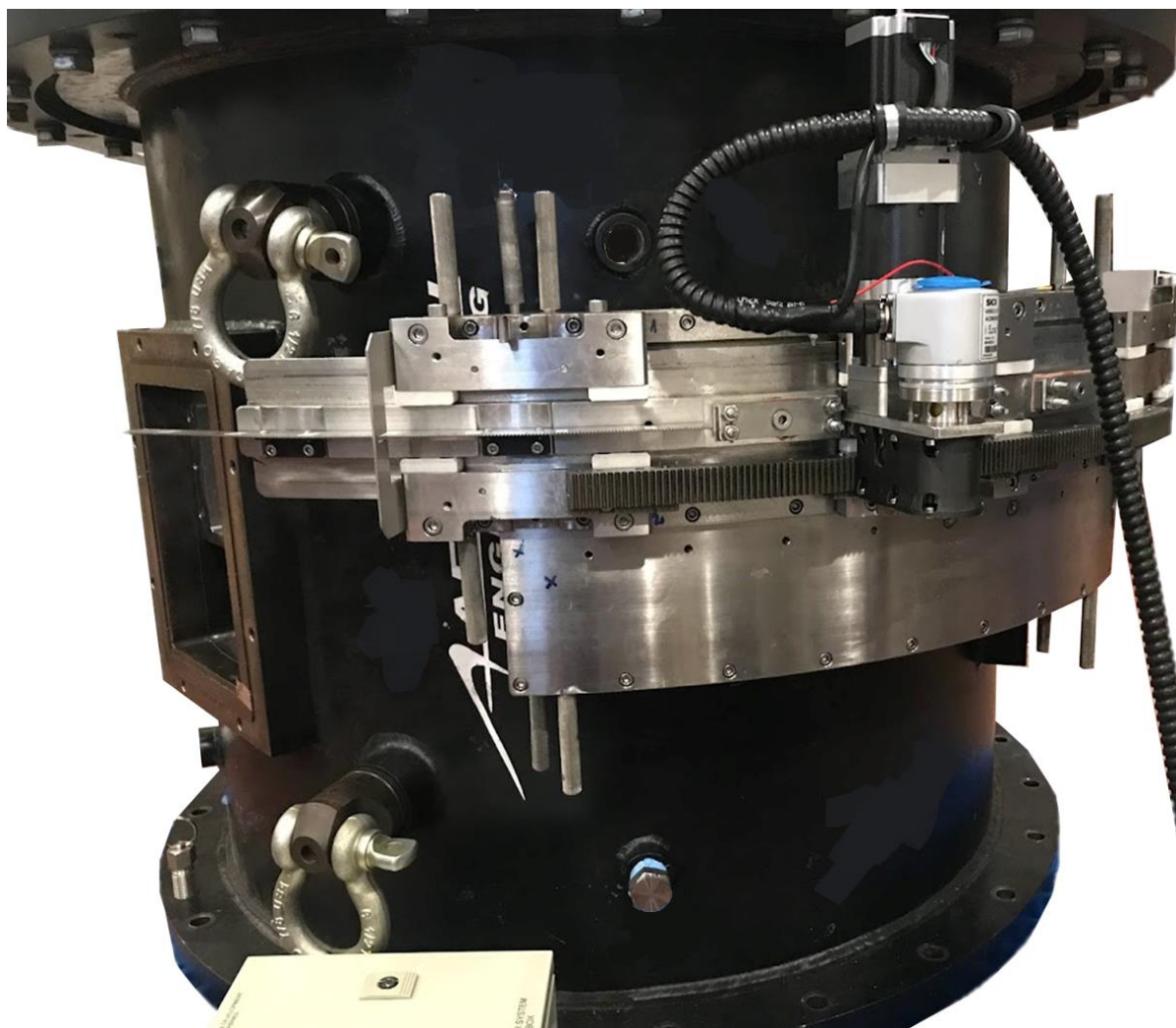


**Fig. 4** Traverse Gear System mounted on BRASTA tunnel

### 3. POSITION CONTROL SOFTWARE

Positioning control can be achieved using DC motor, AC servo motor, stepper motor etc. Applications that require high precision for controlling the position of a given system usually employ stepper motors. Stepper motors are utilized in a variety of applications including surveillance systems, medical applications, telescopes, robots etc. The integrated step movement of the motor can come as an advantage even for the open loop systems that do not require position feedback. Assuming normal functioning of the system, the stepper motors can reach stopping accuracies of up to  $\pm 0.05^\circ$  [7]. Although high accuracy is possible within open-loop control, a malfunctioning of the system can pass undetected, and the accuracy will not be the same. To avoid such pitfalls, a position encoder can be integrated in a closed-loop control system.

The positioning control of the presented traverse gear system is composed out of the following products:

- Nanotech Stepper motor St6018L-3008B
- Reduction planetary gearbox Nanotec GPLE60-2S-40
- Stepper motor controller Leadshine M542
- Position encoder SICK ACM60B-S1KE13x06
- 2 safety micro-switches
- Universal transmitter PR4114, PR Electronics
- Relay Finder 55.34.9.024.0040
- ON/OFF button

To control the angular movement of the assembly, a control board capable of emitting and receiving analog signals in the range of 0-5V or 0-10V continuously and as a pulse train is needed. The control board should be capable of generating two 0-5V signals necessary for the “direction” input and “Start/Stop” input into the motor controller, and one pulse type signal with highs in the range of 4.5-5V and lows between 0-0.5V. The motor controller is by default in start mode, this means if no signal is transmitted to the “Enable” pins, the motor is powered on. Keeping the motor powered on for long periods of time will allow heating of the motor components that are required to be kept below 70°C. A good practice for using the assembly is to power the motor only when a movement is required, otherwise the motor should be powered off.

As for the position given by the encoder, a PR4114 universal transmitter is used to convert the output of the encoder (4-20mA) into voltage output (0-10V), meaning movement in the range 0 to 30 degrees. The transmitter is essential to use the National Instruments PXIe 6363 module available at PETAL as control boards to read the data and send the necessary inputs.

An automatic control software has been developed using LabVIEW and the user interface is presented in Figure 5. The software reads continuously the position provided by the absolute position encoder and adjust in real time the speed and direction of the motor in order to provide a smooth start/stop of the assembly.

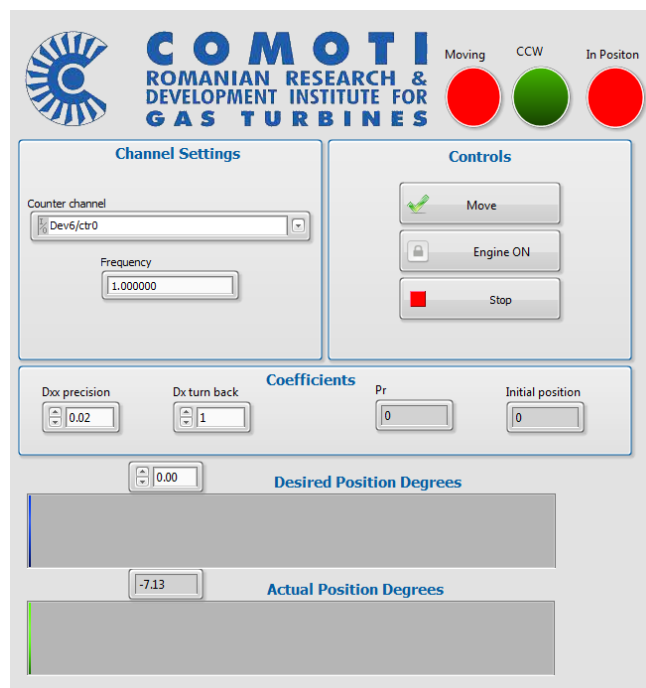


Fig. 5 User interface of automatic control software

The user must select the channel of the control board used to generate pulse train frequency in the range of 0-5V necessary for the movement of the motor. There are 3 LED in the upper right part of the UI which shows to the user the state of the assembly. The user can manipulate the positioning accuracy from “Dxx precision” coefficient depending on the needs of the application (the precision should not exceed the default value because the system is limited by the precision of the position encoder and the precision of reading the analogue signal converted by the PR). The software is designed to move the assembly to the desired position all the time from the same direction, thus if the desired position is smaller than the actual position of the assembly, the software will go back 3° (1 from “Dx turn back” translates to 3° on the assembly) further than the desired position, then change direction and move to the desired position.

The user can select the desired position of the assembly by manipulating the blue slider, or by entering a value into the control number box above the slider. The limits of positioning are between 0°-30° and the user can see live the actual position of the assembly on the green slider.

To start the movement of the assembly to the desired position the user needs to press the button “Move” and wait for the assembly to reach the desired position. When the user does not wish to move the assembly, the engine should be turned off from the button (Engine On/Off).

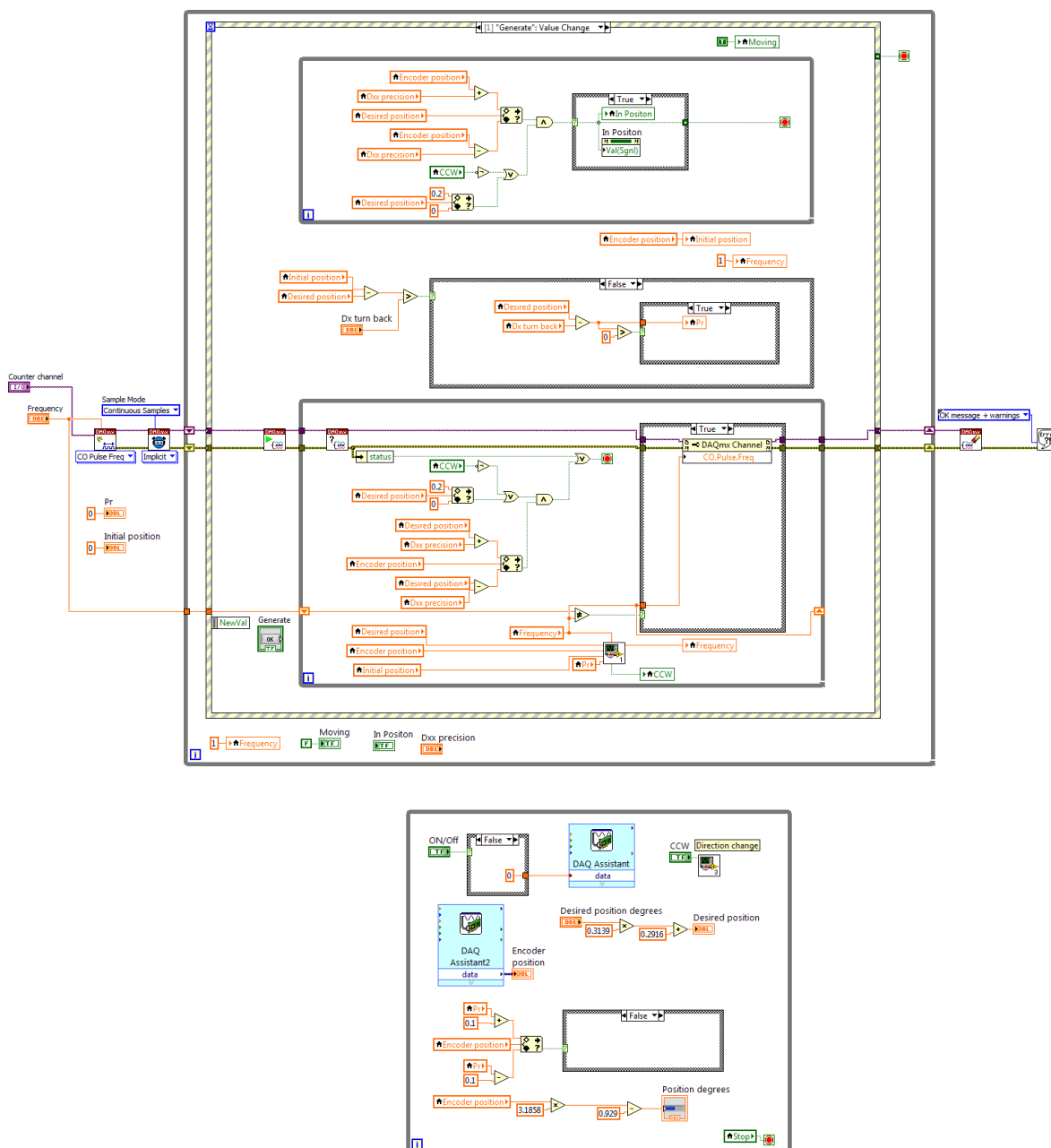


Fig. 6 Block diagram of the positioning control software

The block diagram of the positioning control software is presented in Figure 6. The main VI of the software is composed out of 2 while loops and 2 subVIs. The bottom while loop controls the direction input of the motor, Power On/Off and records the encoder position. The direction is controlled through a separate subVI to minimize the size of the block diagram. The same loop also contains coefficients which are used in the control laws of the stepper motor.

The upper while loop integrates the movement of the stepper motor. It generates a pulse train frequency output using a digital counter to provide the necessary pulses to the engine controller. The starting and stopping of the pulse generation is handled by an event case structure. Because of the nature of the event case structure, during the run of the software it does not take any CPU resources until an event is triggered. The button “Move” presented in the visual interface of the program triggers the “Generate” event, which is also shown in Figure 6. This event enables the generation of voltage pulses in the range of 0-5V. The frequency of these pulses, which relates directly to the speed of the stepper motor, is controlled through another subVI. This subVI contains all the control laws needed to accelerate and decelerate the engine according to its real-time position transmitted by the absolute position encoder.

The event structure can be triggered only by a user generated event. For working around this problem, a “value signalling” property node was used. This specific property node sets the value of a control and causes LabVIEW to generate an event as if the user had interactively changed the value of the object. “In position” control variable is manipulated through this type of property node in order to generate the “In position” event which stops the digital counter and halts the generation of the pulse train.

#### 4. EXPERIMENTAL METHODS

The Traverse device alone just allows for movement in one degree of freedom. However, probes can be mounted on mechanisms capable of providing yaw and radial motion controlled by stepper motors, while the probe itself can obtain data for different pitch directions. PETAL has already designed this mechanism and implemented it in the Small Turbine Aerothermal Rotating Rig (STARR), obtaining satisfactory results at a wide range of operating conditions.

The traverse mechanism combined with the Traverse gear system allows  $-45^\circ$  to  $45^\circ$  yaw, full span radial, and  $-30^\circ$  to  $30^\circ$  pitch wise flow field measurements (see Figure 7 a). The traverse is designed to allow for multiple types of probes, providing measurements of temperature and pressure, flow velocity and flow direction [8].

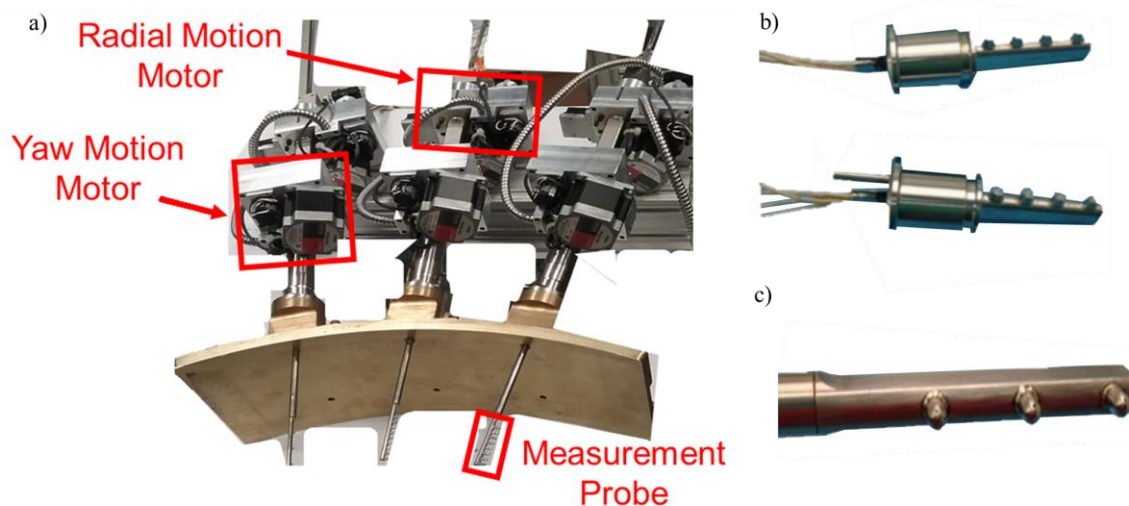


**Fig. 7 a) Traverse mechanism used for measurements at different spatial locations, showing the motors used for radial and yaw motion, b) Thermocouple rake probes c) 5- hole rake [8]**

The BRASTA test section has space claim for a single-stage turbine, allowing testing of stators and/or rotors in a stationary frame. The traverse slots are located downstream of the stator and/or rotor geometries test article. The stepper motors provide a resolution of 0.003 mm in the radial direction and  $0.015^\circ$  in yaw [9]. Since the entire assembly is moving together, all distances are measured in a local system of coordinates, facilitating the calculation of the position of the probes. There are three major probes that will be used in the new Traverse system. Those are five-hole probes for the measurement of velocity and angles, hotwire anemometers for the measurement of velocity fluctuations, and thermocouples for temperature measurements.

All these probes have been already tested and validated in multiple test campaigns in static positions, except for five-hole probes, that have also been implemented in the traverse device. Examples of these probes are shown in Figure 7 b and c.

Five-hole probes measure velocity and flow angle based on pressure differences at the entrance of each of the orifices. The size and separation of both the holes and the heads (in the case of rake configurations) has been optimized based on CFD. Characterization on how the flow interacts with the probe is essential to verify there is no significant change in the flow due to the presence of the probe itself.

Hotwire anemometers measure velocity based on the fluctuation in temperature of a heated wire located in the flow. Convection is the major mechanism for heat transfer and therefore a correlation can be obtained between velocity of the flow and rate of cooling in the hotwire.

Thermocouples are the most common device in terms of temperature measurement. They are inexpensive and easy to manufacture. Type K thermocouples (made of Chromium and Alumel) are, once properly calibrated, capable of measuring accurately temperatures in a linear trend, which eases the postprocessing of the data. Additionally, they show almost negligible drift on the readings between tests, due to the wide range of operating temperature (up to 1250 °C)

## 5. CONCLUSIONS

This paper has presented an automated mechanical module, Traverse Gear System, for three probes positioning inside wind tunnels. The module has been designed to eliminate leakages and to be able to support up to 7 barA of pressure and vacuum conditions. The Traverse Gear System can withstand temperatures of up to 500K. The system can be used to move circumferentially three probes inside the testing section of BRASTA wind tunnel from Purdue University, and ultimately perform a matrix with the acquired data to do a thorough characterization of the fluid flow conditions in subsonic, transonic, and supersonic speeds. The assembly is made from 3 distinct components to provide full mobility across a 0°-30° range. The Probe Carrier can accommodate the 3 measurement probes positioned at 12° angle one from another. An automated software has been developed in LabVIEW which moves and tracks in real-time the position of the assembly and makes corrections to achieve high positioning accuracy of up to 0.06°. The assembly has been tested in-house on a mock-up of the wind tunnel and the leakages have been determined under pressure and vacuum conditions. The Traverse Gear System has achieved its goal and provided small static and dynamic leakages of the probes. The system has integrated several innovations that can make the scope of an international patent.

## REFERENCES

- [1] Amend, J., Povey, T. (2022). Ultra-Compact Traverse System for Transonic Annular Cascade; Proceedings of Global Power and Propulsion Society; ISSN-Nr: 2504-4400; GPPS-TC-2022-0017
- [2] BRASTA WIND TUNNEL <https://engineering.purdue.edu/PETAL/facilities>
- [3] Blair, M. F., Bailey, D. A., and Schlinker, R. H. (October 1, 1981). "Development of a Large-Scale Wind Tunnel for the Simulation of Turbomachinery Airfoil Boundary Layers." ASME. *J. Eng. Power.* October 1981; 103(4): 678–687. <https://doi.org/10.1115/1.3230790>
- [4] <https://en.nanotec.com/products/560-st601813008-b>
- [5] <https://en.nanotec.com/products/907-gple60-2s-40-f87>
- [6] <https://www.sick.com/cn/en/encoders/absolute-encoders/acm60/acm60b-s1ke13x06/p/p371348>
- [7] Oriental Motor; The Powerful Ability of Highly Reliable Stepper Motors; <https://www.orientalmotor.com/stepper-motors/technology/pdf/everything-you-need-to-know-about-stepper-motors.pdf>
- [8] Cuadrado, D. G., Aye-Addo, N., Andreoli, V., Bhatnagar, L., Lozano, F., Fisher, J. M., ... & Johnson, D. (2019). Purdue Small Turbine Aerothermal Rotating Rig (STARR). In *AIAA Propulsion and Energy 2019 Forum* (p. 4004).
- [9] Bhatnagar, L., Paniagua, G., Cuadrado, D. G., Aye-Addo, P. A. N., Castillo Sauca, A., Lozano, F., & Bloxham, M. (2022). Uncertainty in High-Pressure Stator Performance Measurement in an Annular Cascade at Engine-Representative Reynolds and Mach. *Journal of Engineering for Gas Turbines and Power*, 144(2).

# SHORT COMMUNICATION ON ADDITIVE MANUFACTURING TECHNOLOGY USED FOR AXIAL GAS TURBINE ROTOR BLADE

Valeriu VILAG<sup>1</sup>, Cristian DOBROMIRESCU<sup>1</sup>, Alexandru HANK<sup>1</sup>, Cosmin SUCIU<sup>1</sup>, Razvan NICOARA<sup>1</sup>, Mihai VLADUT<sup>1</sup>, Tiberius FRIGIOESCU<sup>1</sup>, Alexandru PARASCHIV<sup>1</sup>

Received: 21.11.2022

Accepted: 22.12.2022

Published: 22.12.2022

**Copyright:** The article is an Open Access article and it is distributed under the terms and conditions Creative Commons Attribution (CC BY) license (<https://creativecommons.org/licenses/by/4.0/>).



**ABSTRACT:** The paper is just a short overview of using additive manufacturing technology for realizing high loaded parts like axial gas turbine rotor blades. Since the focus is on the technology, an existing blade from TV2-117A helicopter engine was selected as reference to avoid design issues. There are tackled sequentially the creation of 3d model of the blade, actual printing, post-processing, testing in laboratory and functional tests on real engine at nominal speed of rotation, 12000rpm. The conclusions state that additive manufacturing technology is really promising for future use in gas turbine parts, but many further investigations must follow especially for aviation purposes.

**KEYWORDS:** turbine rotor blade, 3d printing, functional test

## 1. INTRODUCTION

Additive manufacturing technology or 3d printing gain spectacular development in the 21<sup>st</sup> century due to multiple achievements in computer, optics (LASER) and material development. As in other domains, the increasing power of computers made possible the fine discretization of the models as well as the generation of complex geometry for the needed supports. For advanced gas turbines blades, the technology already appears as an option [1] mainly for development purposes, as shown in Figure 1 which represents a 2022 extension of older evolution prediction from the 80's.

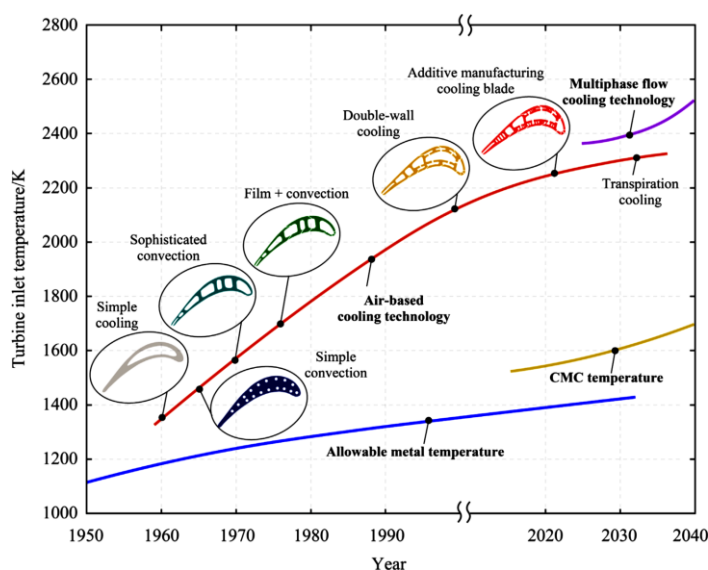
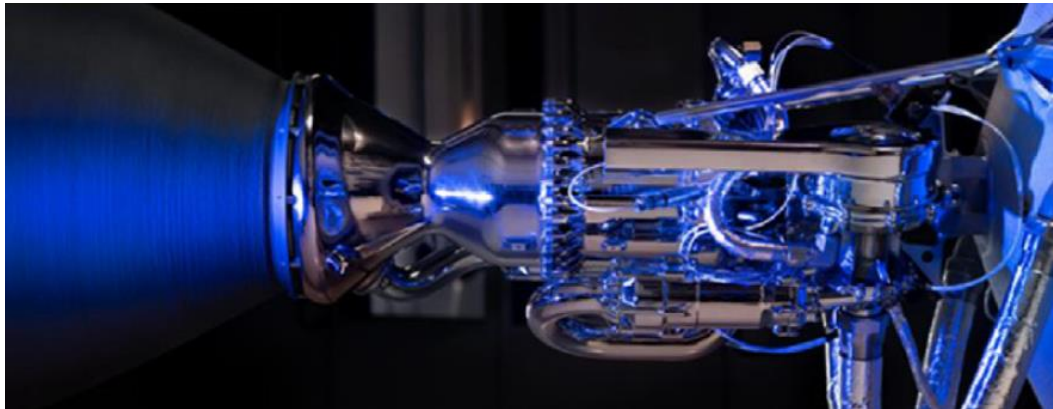


Fig. 1 Evolution of turbine blade technology [1]

<sup>1</sup> Romanian Research and Development Institute for Gas Turbines COMOTI

Other examples of using this relatively new technology include critical parts from rocket engines like the injection nozzles and combustion chamber [2, 3], Figure 2.



**Fig. 2 Printed rocket engine nozzle and combustion chamber [3]**

From operational point of view, it seems that Siemens is the one of most advanced company since they are already using gas turbine printed blades, Figure 3, on industrial 13 MW application [4].



**Fig. 3 Industrial gas turbine printed blades [4]**

Many other companies invest in additive manufacturing, General Electric from USA being just another big actor who is also investigating the use of additive manufacturing technology for gas turbine blades in collaboration with Avio Aero from Italy, figure 4 [5].



**Fig. 4 General Electric GE9X additive manufactured blades [5]**

The work in this paper came in the context of additive manufacturing emerging technology which became available in COMOTI for metals several years ago and many studies have been made since [6,7]. The purpose is to evaluate if this new technology is ready applicable to high precision and high loaded, stress due to high speed of rotation and temperature, parts like axial gas turbine blades.

Since the focus was only on the technology, the gas-dynamic and mechanical design of the blade were replaced by other processes targeted on an existing gas turbine, namely TV2-117A, a helicopter turboshaft used for research purposes since many years.

The overall work logic consisted in selecting an individual gas turbine blade, precision scanning of the selected blade, 3d CAD (Computer Aided Design) model creation, definition of additive manufacturing parameters, actual manufacturing of the blade, post-processing operations, mounting onto the gas turbine assembly, testing in laboratory and in real conditions. Several loops were integrated into the work logic to have the desired results, but they were based on simple engineering tools not on sophisticated algorithms.

In comparison to other studies, the current one proposes the complete elimination of machining on the obtained parts reducing thus even more the manufacturing time and costs.

## 2. INDIVIDUAL AXIAL GAS TURBINE BLADE

We mention again that the focus is on testing the technology, so, the selected blade, Figure 5, is from the second stage of free power turbine of the TV2-117A turboshaft engine powering the Mi8 helicopter, one of the most produced helicopters in the world. Nevertheless, this blade incorporates all the design features of modern gas turbine blades, fir tree root mounting on the blade and labyrinth seal outer shroud, except cooling, since it doesn't need it as last turbine row.

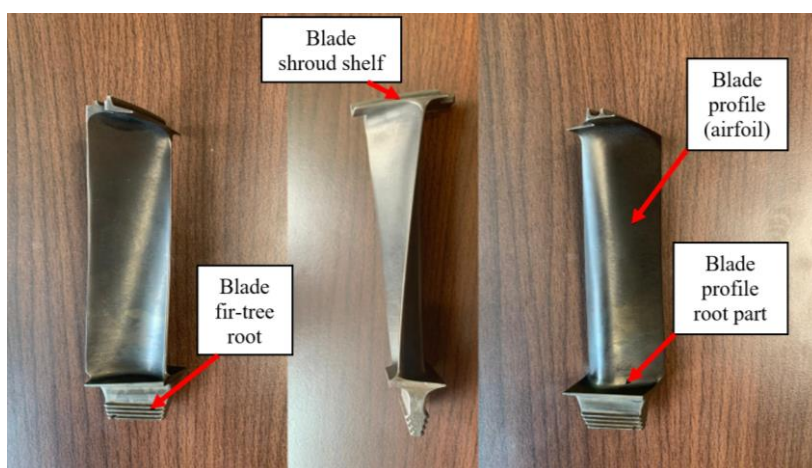


Fig. 5 Original individual axial gas turbine blade

The blade was scanned using high precision devices, GOM-Zeiss ATOS 5M 3d optical scanner and LC15Dx Nikon laser scanner mounted on a Nikon Altera 10.010.8 3d CMM (Coordinate Measuring Machine), with declared resolution of 1.9 microns. The most difficult part for interpretation was the fir-tree root, where multiple parallelism of the edges, cylinders, and planar faces as well as linear spacing had to be precisely determined, Figure 6. Thus, the entire CAD model of the blade was created first in GOM Inspect and then in CATIA V5 software. Some gas-dynamic and stress calculus were performed to verify from functional point of view the obtained CAD model and relatively good correlation with the engine data was obtained (estimated power of about 750 HP, meaning even distribution of the total of 1500 HP between the two free power turbine stages).

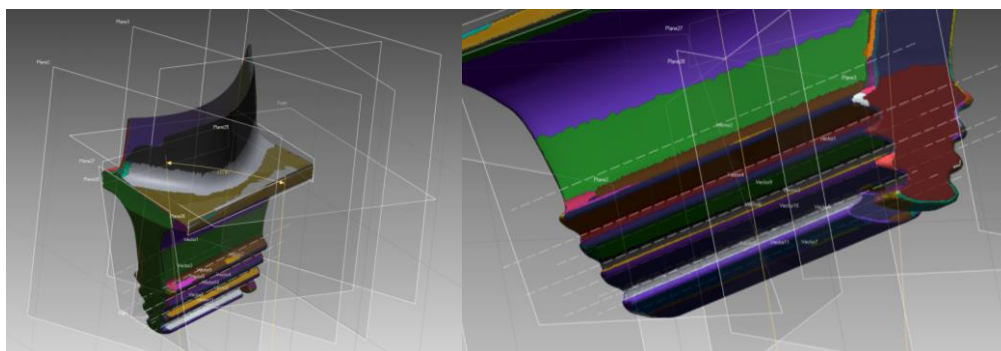


Fig. 6 Surface generation after scanning

### 3. ADDITIVE MANUFACTURING

Additive manufacturing is already common our days but for parts like gas turbine blades which are subjected to high temperature and high rotational speed, one must pay attention to the material that is used and to the printing parameters affecting material properties. On the present study INCONEL 625 was used due to its potential for gas turbine application and DMG MORI Lasertec 30 SLM (Selective Laser Melting) machine due to its freedom of choosing the printing parameters. Some studies have been made before, but they were targeting a blisk like turbine rotor for microjet and turbopump application [6].

After properly choosing the technological parameters to give the desired material properties from density, roughness and rupture stress at room and elevated temperature and from geometrical accuracy point of view [7], many trials were made concerning the positioning of the model in the printing chamber. These trials focused on the fir-tree since here is where the higher geometrical precision is needed, in the order of 3 microns, but also on the airfoil where the precision must be in the order of 0.1mm. The precision of the fir-tree obtained through additive manufacturing was tackled with many versions of scaled/offset fir-tree profiles that were verified with the original disc in place of a caliber. The roughness cannot be compared with the one obtained by grinding but the overall lobes profile can be controlled since the used additive manufacturing technology is sensitive to 3d model change in the same order of 3 microns.

Another important criterion was to reduce as much as possible the supports since they are rather difficult to remove. The final positioning on the machine plate is presented in Figure 7.

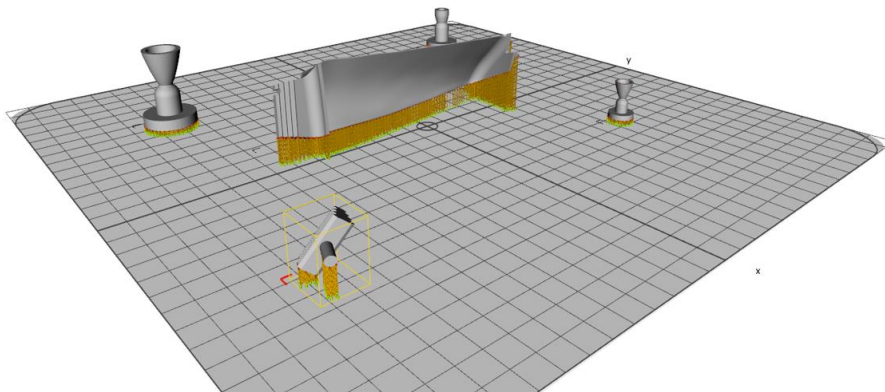


**Fig. 7 Final positioning of the blade (along with other parts in the same job)**

The manufacturing process lasted about 9 hours for each blade (with the manufacturing parameters defined according to [7]) and the results were evaluated first by optical scanning, just like the original blade, Figure 8. The values are acceptable considering also that they include the alignment error of the part into the machine volume (the cloud points were aligned using the four cones features on the machine plate that are used to align the plate into the printing volume, and its flat surface). Some other evaluation consisted in mass and eigen frequency determination, which, in comparison to original blades, gave also satisfactory results (deviation under 10 %; about 11 grams and about 130 Hz).

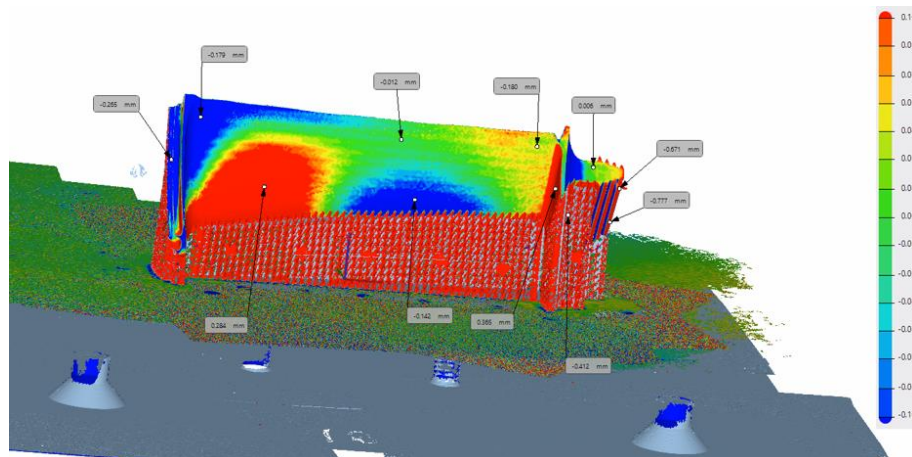


**Fig. 8 Scan result for one of the printed blades**

#### 4. POST-PROCESSING AND MOUNTING

Post-processing and finishing operation included: removal from the machine plate, removal of supports, hand finishing of the surface. We just mention that hand finishing was performed using special low abrasive multi-layer disks which allow fine control when removing the supports since when reaching the blade, the texture of the material consumes a lot from the abrasive layers.

Figure 9 presents some of these operations but is important to mention that machining was not performed on the manufactured blades nor heat treatment or other similar processes that may affect the geometrical and dimensional accuracy of the part.

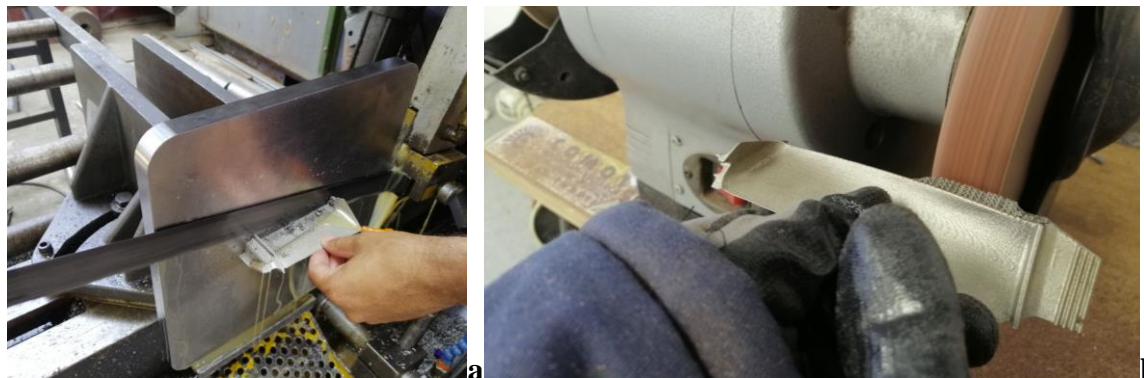


Fig. 9 Removal of one blade from the machine plate (a) and removal of supports (b)

Two manufactured blades were mounted onto the rotor of a modified TV2-117A working on alternative fuels [8]. To reduce any additional unbalance to the existing rotor, due to mass difference in comparison to the replaced blades (about 11 grams meaning minus 10%), the two blades were mounted in opposition, Figure 10, and the entire gas-turbine was re-assembled and mounted on the test bench.

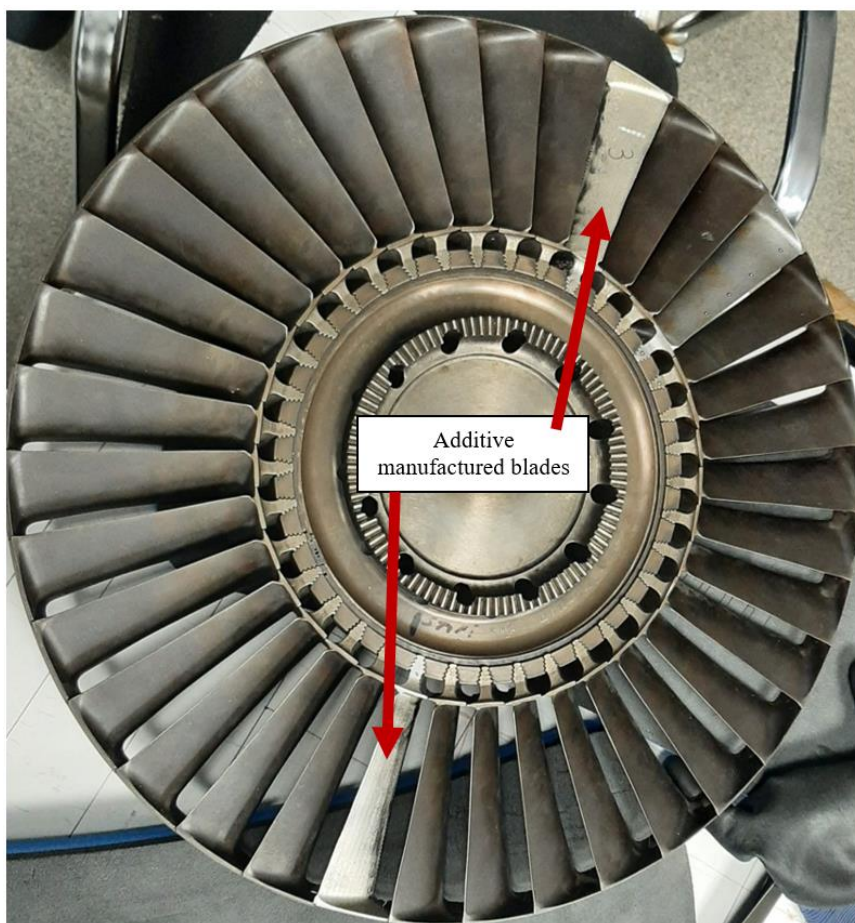


Fig. 10 Two printed blades mounted on the rotor

### 5. TESTING

Before spinning the turbine with the two manufactured blades at nominal speed of 12000rpm, some more attention was paid to the fir tree assembly feature. Several samples of the interest area were manufactured and subjected to load and temperature on an Instron 8802 universal testing machine according to Table 1. Test parameters were chosen in accordance with EN ISO 6892-2:2018 Metallic materials — Tensile testing — Part 2: Method of test at elevated temperature. The maximum test temperature was selected considering the maximum regime of TV2-117A helicopter engine and the corresponding parameters in front of the second stage of the free power turbine.

**Table 1. Experimental matrix “Fir-Tree root”**

No.	Sample	Load [kN]	Temperature [°C]	Load speed [N/s]	Observations
1	Sample 1	82.5	30	50	This result is to be considered as reference for room temperature tests
2	Sample 2	11.5	30		The preload test is performed at different temperatures. After each test the sample is unloaded, and the temperature is increased.
3			360		
4			460		
5			560		
6			69.1		
7	Sample 3	11.5	30		The preload test is performed at different temperatures. After each test the sample is unloaded, and the temperature is increased.
8			360		
9			460		
10			560		
11	68.8	560	The tensile load is gradually increased until sample breaking point.		
12	Sample 4	11.5	30		The preload test is performed at different temperatures. After each test the sample is unloaded, and the temperature is increased.
13			360		
14			460		
15			560		
16			71.5		

Figure 11 presents the CAD 3d model of the samples containing the blade root (fir-tree) and the load vs. deformation of the samples tested at 560° Celsius. Sample 1 is missing because its only purpose was to have some reference values for room temperature tests.

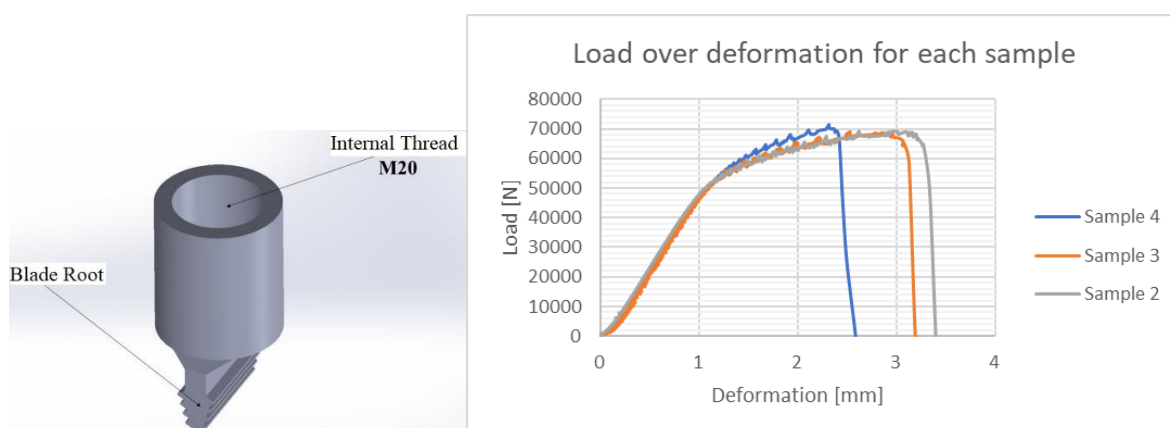


**Fig. 11 Test sample CAD model and load versus deformation for each preloaded sample**

For all the test samples it was observed that the sample did not broke on the lobes of the fir tree root, meaning that the lobes can withstand the centrifugal load of the blade, figure 12. More, the obtained loads at fracture were high enough considering the calculated centrifugal force acting on the blades, 70kN compared to 26kN, and creep effects.

The differences between the samples are considered small and, in the region, where it almost doesn't matter. They can be due to many factors like small differences between samples, usage of the counterpart acting as disk, small difference of the test temperature etc.



**Fig. 12 Test specimen for fir-tree root after fracture at high temperature**

Test of the gas-turbine equipped with the two manufactured blades on the rotor of the second stage of the free power turbine were performed in the envelope permitted by the existing testing facility. A rotational speed of 12000 rpm (nominal according to the engine manufacturer) and about 400 Celsius degrees at the envisaged blades were obtained with zero load on the free power turbine. Vibration of the engine remained in safe margins (amplitude under 12 mm/s) meaning that the mass difference between the additive manufactured blades and the replaced ones is small enough and the balancing of the free power turbine rotor is unaffected.

## **6. CONCLUSIONS**

Additive manufacturing technology is very promising even for high demanding parts like gas turbine blades subjected to high rotational speed and high temperatures. The manufactured blades were post-processed just for supports removal, meaning that from geometrical point of view there is no need for additional machining, and tests on modified helicopter engine have been performed.

From zero to nominal rotational speed of two manufactured blades mounted on the original disk, vibration was in safe margin, meaning that any mass and/or eigen frequency difference between the additive manufactured blades and the replaced ones did not affect the overall balancing of the free power turbine rotor

Future research steps include functional tests with the current configuration with only two additive manufactured blades at nominal working regime (rotational speed, load, pressure, and temperature), realization of complete crown of new blades and functional tests as well as shape and technological optimization of the blade itself to use the advantages of the additive manufacturing technology. As goals for optimization there will be used, among others, reducing the weight of the blade, internal passages for cooling to allow the use of materials with lower permissible temperature and hence cheaper, manufacturing time reduction etc.

Benefits of heat treatment of the parts (even Hot Isostatic Pressing) and other type of inspection besides optical (like X-Ray) will be also investigated in the future.

Of course, that for aviation purposes at least, the technology must be further investigated, and any additive manufactured blade should be accompanied on the building plate with many samples for proper evaluation of mechanical and gas-dynamic performances and even for traceability issues of each blade.

As a final remark, we may say that the presented work represents a valuable tool for maintenance activities in case one cannot find original replacement blades since all can be seen as reverse engineering.

## **ACKNOWLEDGEMENT**

The presented study was performed in the frame of 3dBlade project (COFUND-ERANET MANUNET III-3dBlade, UEFISCDI, ctr. 97/2019) and TURBOPROP Nucleu Program 2019-2022 within COMOTI Romanian Research and Development Institute for Gas Turbines.

## REFERENCES

- [1] Unnikrishnan U., Yang V., (2022). A review of cooling technologies for high temperature rotating components in gas turbine, *Propulsion and Power Research* 2022;11(3):293e310, <https://doi.org/10.1016/j.jprr.2022.07.001>
- [2] Karakurt I., Lin L., (2020). 3D printing technologies: techniques, materials, and post-processing, *Current Opinion in Chemical Engineering* 2020, 28:134–143, <https://doi.org/10.1016/j.coche.2020.04.001>
- [3] Relativity Space — Relativity Space, (n.d.). <https://www.relativityspace.com/terran>, (accessed on 15.11.2022)
- [4] Anderson M., (2019). New metals shine in 3D printers: with novel materials, 3D printing can build more products - [News]. *IEEE Spectr* 2019, 56:9-10, <http://dx.doi.org/10.1109/mspec.2019.8678423>
- [5] [www.ge.com](http://www.ge.com) (accessed on 19.12.2022)
- [6] Dobromirescu C., Vilag V., (2019), Additive Manufacturing for a Turbopump rotor, *TURBO scientific Journal*, vol. VI (2019), no. 2, ISSN: 2559608X, ISSN-L: 1454 2897, [http://www.comoti.ro/ro/jurnalul\\_stiintific\\_turbo.htm](http://www.comoti.ro/ro/jurnalul_stiintific_turbo.htm)
- [7] Matache G., Vladut M., Paraschiv A., Condruz R., (2020), Edge and corner effects in selective laser melting of IN 625 alloy, *Manufacturing Review*, Volume7 2020, Article Number 8, DOI: 10.1051/mfreview/2020008
- [8] Vilag J., Vilag V., Puscasu C., Nicoara R., Calugaru M., (2019). Numerical Simulation of Alternative Fuels Combustion in Gas Turbines, Application of mathematics in technical and natural sciences, Book Series AIP Conference Proceedings, Volume 2164, Article Number 070003, DOI: 10.1063/1.5130823

# EXPERIMENTAL INVESTIGATION OF AXIAL POWER TURBINE IN TURBOSHAFT APPLICATION

Alexandru HANK<sup>1</sup>, Valeriu VILAG<sup>1</sup>, Răzvan Marius CATANĂ<sup>1</sup>, Gabriel DEDIU<sup>1</sup>,  
Mihai Cornel TĂRĂBÎC<sup>1</sup>, Cosmin Petru SUCIU<sup>1</sup>, Cristian DOBROMIRESCU<sup>1</sup>

Received: 15.11.2022

Accepted: 20.12.2022

Published: 22.12.2022

**Copyright:** The article is an Open Access article and it is distributed under the terms and conditions Creative Commons Attribution (CC BY) license (<https://creativecommons.org/licenses/by/4.0/>).



**ABSTRACT:** This paper presents the methodology and results of experimental studies on axial turbine performance regarding the work of design, testing, and post-processing of collected data. The study was made on an axial gas turbine designed entirely by the Romanian Research and Development Institute for Gas Turbines COMOTI and is intended to serve as the third power turbine stage of a 1500 kW industrial turboshaft. Furthermore, this is the first complete experimental turbine assembly designed and manufactured entirely in Romania. For testing purposes, a Klimov TV2-117A gas generator was coupled to the experimental turbine to ensure the thermodynamic and chemical properties of the flue gas at its inlet section. The turbine was tested in such a way as to collect all the necessary data for obtaining the turbine performance at various regimes. The results show a significant increase in the turbine power output, up to 248.4 kW at 85% of the maximum gas generator speed (NGGmax=21200 rpm).

**KEYWORDS:** Gas turbine, turboshaft, turbine testing, turbine power output

$NGG$	-	Gas generator speed
$NTP$	-	Free turbine speed
$P$	-	Power
$T_0$	-	Ambient static temperature
$T_2^*$	-	Compressor exit total temperature
$T_3^*$	-	Combustion chamber exit total temperature
$T_4^*$	-	Experimental turbine inlet total temperature
$T_{45}^*$	-	Experimental turbine exit total temperature
$P_0$	-	Ambient static pressure
$\Delta P_{10}$	-	Bell-mouth inlet differential pressure
$P_2$	-	Compressor exit static pressure
$P_4^*$	-	Experimental turbine inlet total pressure
$P_{45}^*$	-	Experimental turbine exit total pressure
$c_{sp}$	-	Specific fuel consumption
$RH$	-	Relative humidity
$Vb_{MO}$	-	Gas generator axial vibration
$Vb_{MV}$	-	Gas generator radial vibration
$Vb_{TO}$	-	Free turbine axial vibration
$Vb_{TV}$	-	Free turbine radial vibration
$T_{UITP}$	-	Free turbine oil temperature

<sup>1</sup> Romanian Research and Development Institute for Gas Turbines COMOTI

## 1. INTRODUCTION

Turboshaft engines are generally described as having a power turbine in their composition and are usually used to drive the blades of rotary wing aircrafts, marine propellers, or electrical generators. Most of them are two-spool engines with a free turbine located downstream of the gas generator that is responsible for converting the remaining energy of the burnt gas into shaft power. The main advantage of this configuration is that the free turbine is not mechanically connected to the gas generator, so its speed is independent. Thus, the two turbines can operate at different shaft speeds. This is essential while operating with varying loads such as for the helicopter rotary blades system [1].

The TV2-117 two-spool turboshaft engine finds its application as the powerplant of Mil Mi-8 and Mil Mi-14 helicopters and is known as one of the most popular helicopters powerplants, with over 100 million hours in service and about 23.000 engines produced [2]. According to the service manual [3], TV2-117A specifications at the main regimes are listed in table 1.

**Table 1. TV2-117A specifications**

Regime [rpm]	P [HP]	$c_{sp}$ [g/HP/h]	NGG [%]	NTP [%]	$T_{3max}$ [°C]
Takeoff	1500	275	98.5	93 - 1	850
Nominal	1200	295	96	95 ± 2	790
Cruise	1000	310	94.5	95 ± 2	750
Idle	-	max 100 kg/h	64 +2/-1	45 ± 10	600

The reference values for the shafts speeds of TV2-117A are  $NGG_{100\%} = 21200$  [rpm] for the gas generator and  $NTP_{100\%} = 12000$  [rpm] for the free turbine. Other important parameters available in the literature are the compressor pressure ratio and the mass flow rate. The compression ratio provided by Guston Bill in both [4] and [5] is 6.6 at 21200 rpm, while Varga Bela obtained a value of 6.24 compression ratio for maximum net work using the model presented in ref. [6]. The mass flow rate is not as well defined in the literature since it ranges between 8.4 kg/s for maximum speed according to [4] and 7.4 kg/s for 99.11% NGG speed, obtained in the experimental investigation presented in ref. [7]. Some experimental studies related to this particular engine describe a more detailed correlation between the power output and NTP speed at intermediate regimes that are not listed in the manual. Catană R.M. et al. [7] obtained a maximum power of 1027 kW at 99% of NGG speed, which is lower than the power claimed in the manual, but is conceivable considering the age of the tested engine.

In this application, the free power turbine of TV2-117A has been replaced with the experimental turbine developed by COMOTI in order to compare their performances, since the inlet conditions for both are very similar. The experimental turbine is an axial blisk, and it was designed to serve as the third stage of a 1500 kW power turbine industrial turboshaft that operates at a nominal speed of 22000 rpm. Both stator and rotor are made of steel alloys (X6CrNiTi18-10 for the stator and X19CrMoNbVN11-1 for the rotor) and can withstand temperatures up to 550 °C at a maximum speed of 16000 rpm. These materials were selected considering the financial costs and ease of manufacture. The lubrication system is based on two journal hydrodynamic bearings that need a mass flow of 80 kg/min of lubrication oil at temperatures between 60°C and 90°C and pressure between 2.5 and 3.2 bara. The sealing is done by a labyrinth seal which requires compressed air at 1.3 bar to overcome the oil pressure. An isometric view of the experimental turbine assembly is shown in figure 1.a and figure 1.b.

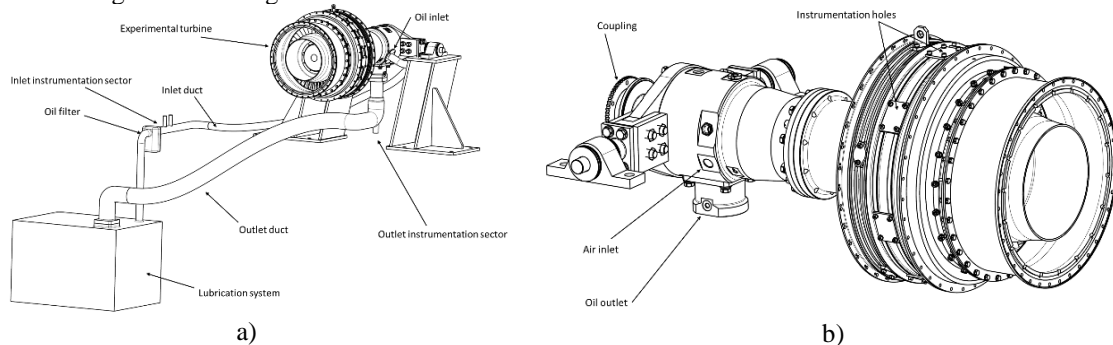


**Fig. 1. a), 1-b) – Experimental turbine assembly**

## 2. EXPERIMENTAL TURBINE AND TV2-117A INSTRUMENTATION

To carry out the study of the experimental turbine performance, proper instrumentation, an acquisition-control system and a dedicated software were needed. A general schematic of the testing installation is shown in figure 2.

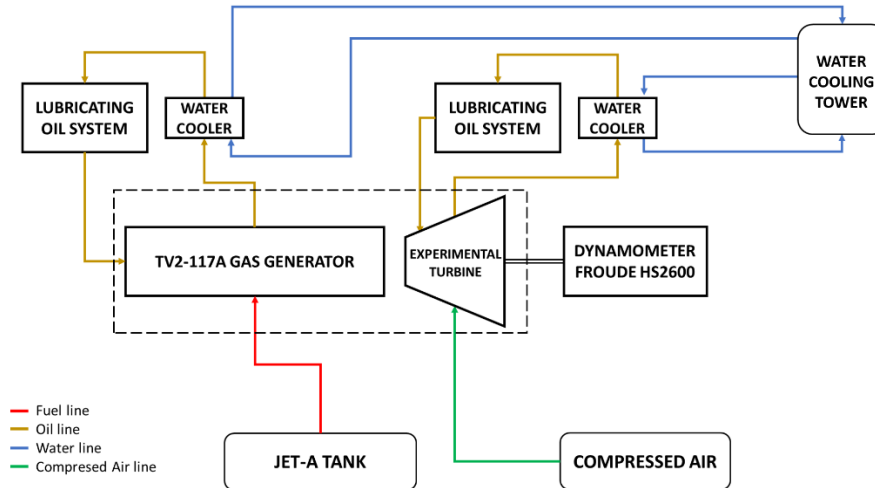


Fig. 2. General schematic of testing installation

The instrumentation was done based on the instructions from the engine manual [3] and the general recommendations presented in ref. [8], and it consists of sensors and transducers that were metrological calibrated before the experimentation campaign.

To determine the atmospheric conditions of the test cell, some parameters are needed, such as the ambient pressure and temperature  $P_0, T_0$  and the relative humidity  $RH$ .

For the air mass flow instrumentation, a differential pressure  $\Delta P_{10}$  was measured in the section of the bell-mouth inlet that was connected to the engine (figure 3-a), then the mass flow was calculated in real-time as a function of the pressure drop and several coefficients that describe the inlet geometry [9]. For the compressor exit section, it was necessary to add a static pressure  $P_2$  probe and two total temperature  $T_2^*$  sensors, and for the combustion chamber exit section, two total temperatures  $T_3^*$  were measured by receiving the signal directly from the engine terminals, each total temperature being an average value of 17 thermocouples measurements at different depths. For the experimental turbine, the total temperature and total pressure were measured at the inlet and outlet sections, as shown in figure 3-b.

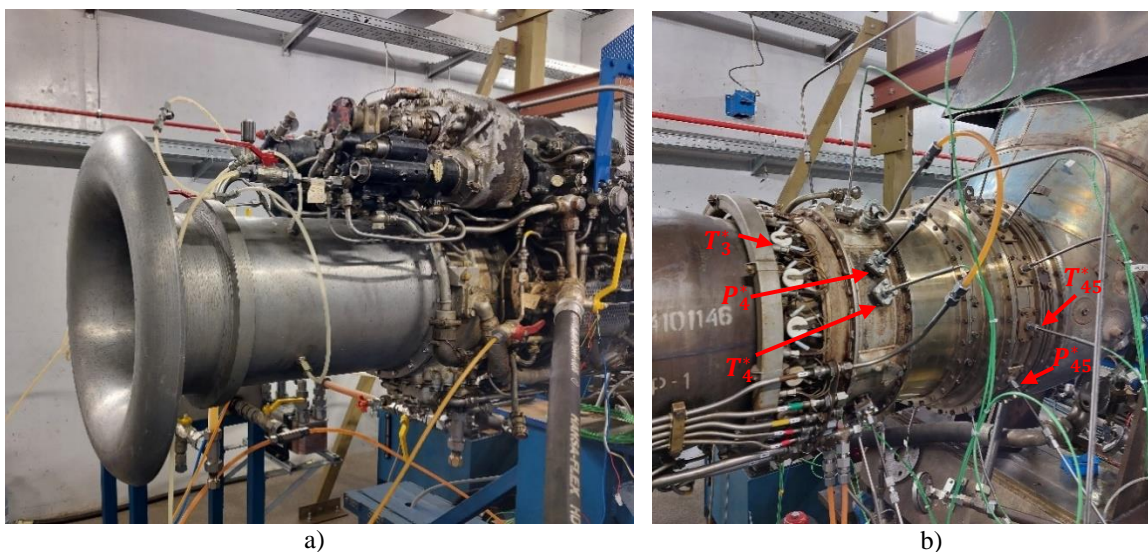
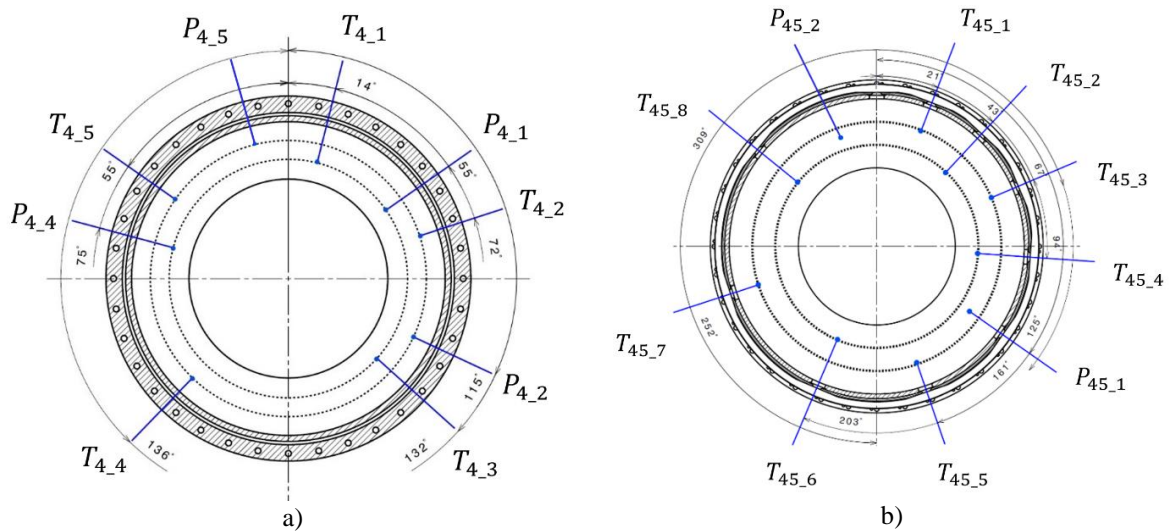


Fig. 3. a) Bellmouth inlet, b) Experimental turbine instrumentation

In the inlet section of the experimental turbine, 5 total temperatures and 4 total pressures were instrumented in different points distributed along the radius and circumference of the annulus section, as shown in figure 4-a. One of the total pressure probes ( $P_{4,3}$ ) was not installed due to the access restriction caused by a lubrication duct of the gas generator. The measuring point of the thermocouples and pressure probes was inserted at 2/3 or 1/3 of the total depth, as shown in figure 4-a). For the exit section, the same principle was applied, but this time 8 thermocouples and 2 pressure probes were installed in order to obtain a better image of temperature distribution downstream the turbine rotor, and the measuring point of the pressure probes  $P_{45,1}$  and  $P_{45,2}$  was inserted at half of the total depth of the flow channel (as shown in figure 4-b).



**Fig. 4. a) Turbine inlet section instrumentation, b) Turbine exit section instrumentation**

For the high range measurement that refers to temperatures, Caom Pascani type K thermocouples were used, those having a measuring domain ranging from 0°C to 1300 °C and a precision of 0.1% of domain. For pressure measurements, the Baker Hughes - Unik 5000 pressure sensors were used, those having an accuracy in full scale of  $\pm 0.04\%$  and a maximum frequency response of up to 3.5 KHz.

To monitor the most important parameters in real-time, a series of sensors were directly connected to the experimental group. The following parameters were measured: the speed of the power turbine NGG, the speed of the free turbine NTP, the axial and radial vibration for the TV2-117A gas generator  $Vb_{MO}$ ,  $Vb_{MV}$  and the axial and radial vibration of the experimental turbine  $Vb_{TO}$ ,  $Vb_{TV}$ .

In addition to the engine instrumentation, a few auxiliary systems were used and instrumented, such as the fuel and oil systems, where both the flow rate and inlet pressures and temperatures were measured.

The shaft power delivered by the experimental turbine was measured using a Froude Hofmann HS2600 dynamometer that was connected to the turbine shaft through a flexible coupling. The turbine shaft was aligned to the dynamometer shaft according to its manual [10]. The total indicated readings recommended by the manual are illustrated in figure 5-a. On the test rig (figure 5-b), the misalignment was reduced to -0.01 mm on the vertical axis and +0.1 mm on the horizontal axis, the distance measured between shafts was 257.9 mm.

On the vertical axis, the alignment was done considering the journal hydrodynamic bearings clearance, which is 0.1 mm according to the technical drawings and measurements.

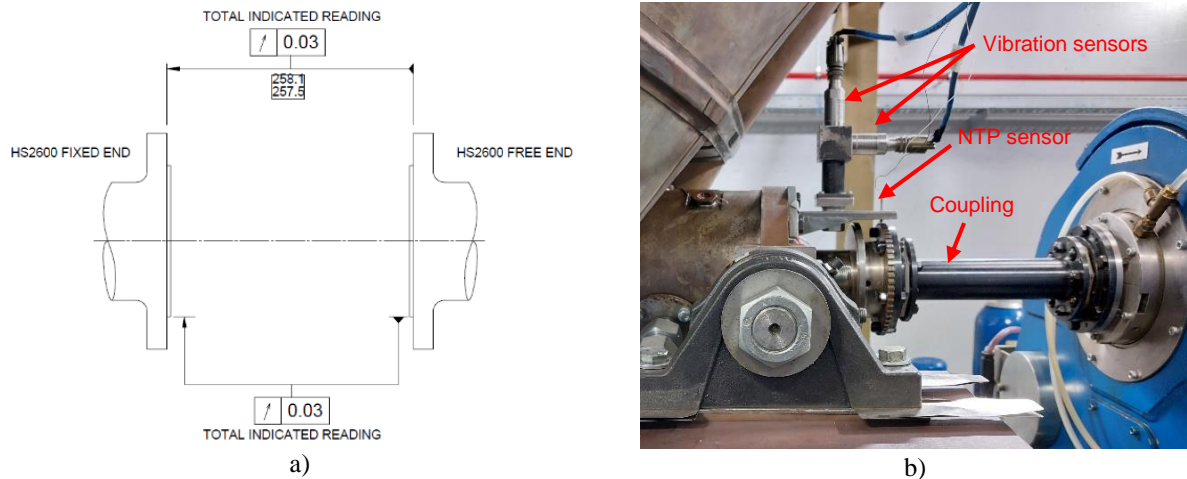


**Fig. 5. a) HS2600 recommended readings, b) Experimental turbine coupled to the dynamometer**

### 3. TESTING PROCEDURE

The test procedure was established in such a way as to obtain the power characteristic lines of the experimental turbine. In gas turbine similarity theory, the characteristic lines are defined by constant reduced mass flow rates that are equivalent to a constant gas generator regime, considering that there are no mass flow variations in the system. By changing the free turbine speed in these conditions, the variation of power with respect to speed can be determined. By plotting the turbine power and the NTP speed, the points for a constant NGG speed should describe a good approximation of a line of constant reduced mass flow rate.

Therefore, for each constant NGG regime, the NTP speed was reduced from the maximum speed until the peak power value could be observed. The NTP speed was decreased with a step of 1000 rpm for high regimes (16000-18000 rpm) and a step of 2000 rpm for low regimes (13600-15000 rpm) using the dynamometer, as shown in figure 6. Measurements were taken for NGG speeds ranging from 13600 rpm (which is the idle regime for TV2-117A) up to 18000 rpm, which is the highest regime for the gas generator, such that the total temperature at the experimental turbine inlet section could not exceed the limitation of 550 °C.

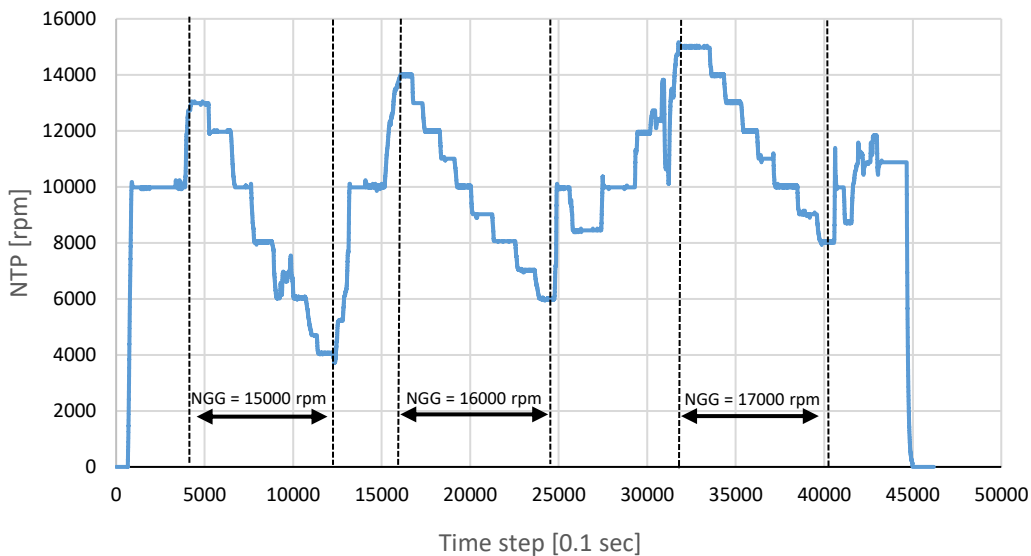


**Fig. 6. NTP variation for 15000 rpm to 17000 rpm NGG regimes**

The tests were performed considering the limitations of the experimental turbine imposed by the materials that it's made of. Additionally, more safety limitations were added, such as the oil temperature and radial and axial vibrations for both the gas generator and experimental turbine (table 2).

**Table 2. Experimental turbine limitations**

Parameter:	NTP [rpm]	T <sub>4</sub> [°C]	T <sub>UITP</sub> [°C]	Vb <sub>MO</sub> , Vb <sub>MV</sub> [mm/s]	Vb <sub>TO</sub> , Vb <sub>TV</sub> [mm/s]
Limitation:	16000	550	90	20	20

#### 4. RESULTS

The maximum power was obtained for the highest tested regime: 248.4 kW at 85% NGG speed. At this regime, the experimental turbine reached a speed of 15000 rpm. In figure 7, the measured power variations for the experimental turbine and TV2-117A engine obtained in ref. [7] can be observed.

Most of the power output of a free turbine is produced, in general, at higher regimes, for example the TV2-117A engine can deliver up to 894 kW at 96% NGG speed and 1118 kW at 98.5% [1], so, for 2.5% of NGG speed, the power is increased by 224 kW. The same characteristic can be observed for the experimental turbine. The difference between the 80% and the 85% regimes is significantly bigger than that between the 75% and the 80% regimes, so it is expected to obtain better performances at nominal speed.

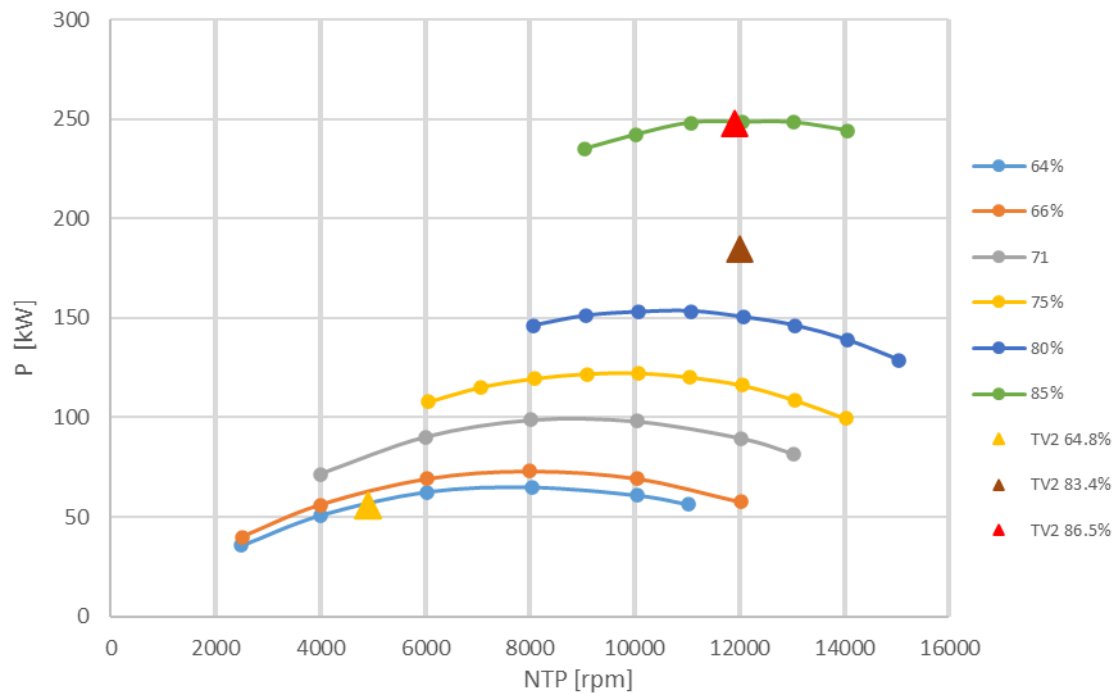


**Fig. 7. Experimental turbine power characteristic compared to TV2-117A free turbine power**

For this campaign, the turbine was tested at the highest regime considering the temperature limitations presented in table 2. As can be seen in figure 8, the turbine rotor blisk shows significant signs of corrosion and high temperature exposure judging by the purple color of the blades, which indicates that the turbine temperature was close to the tempering point of the material. Nevertheless, the NDT defectoscopy analysis by means of penetrating substances has shown no cracks on the turbine blisk.

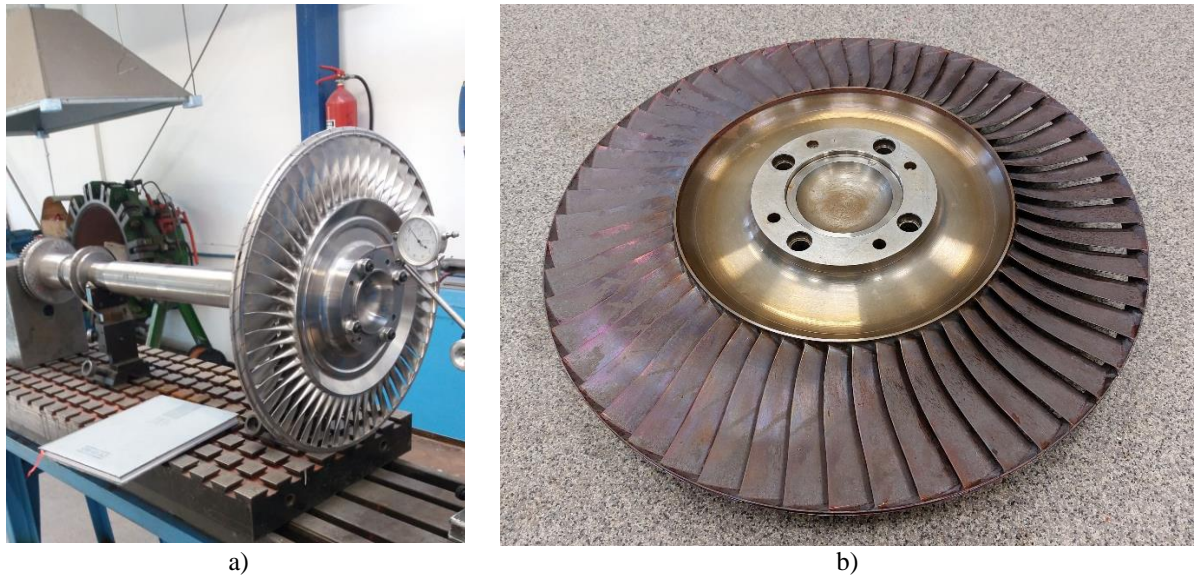


**Fig. 8. a) – Turbine rotor assembly before testing, b) – Turbine rotor blisk after testing**

Comparing those results with the previous experimental campaign on the TV2-117A engine shows that the two turbines have similar performances for the tested regimes (table 3). The main difference between them is that the TV2-117A power turbine speed is regulated at 98%-99% of its maximum speed at high regimes and  $45\pm 10\%$  at idle, while the experimental turbine is not regulated so it can reach higher speeds.

A good comparison between the results obtained in the design phase and the experimental data can be achieved by testing the turbine over its entire operating range, therefore, theoretical performance at the nominal regime is not relevant to the experimental data at this moment. Thus, for future work, improvements in terms of the material the turbine is made of will be made to properly validate the theoretical/CFD results by testing the turbine at the nominal speed.

**Table 3. Experimental turbine and TV2-117A free turbine specifications**

	TV2-117A			Experimental turbine		
	NGG [rpm]	NTP [rpm]	P [kW]	NGG [rpm]	NTP [rpm]	P [kW]
1	13700	4900	55.9	13600	6000	62.4
2	17700	12000	184.7	17000	12000	150.4
3	18300	11900	248.1	18000	12000	248.4

## 5. CONCLUSIONS

The experimental turbine performed as expected within the limits imposed. For higher regimes, both stator and rotor blades should be made of a material that can withstand higher temperatures (up to  $750\text{ }^{\circ}\text{C}$  at nominal speed).

To obtain the universal characteristic of the turbine, the averaged values of total temperatures and pressures at the inlet and exit sections of the turbine must be determined. For this purpose, a suitable averaging technique will be used in future work [11]. In the interest of obtaining a better distribution of total temperature and pressure based on experimental data, the measurements should be taken in more points distributed along the radius and circumference of the inlet and outlet sections of the turbine. A solution for the inlet section instrumentation is presented in ref [8] and it consists of integrated pressure probes and thermocouples in the turbine stator blades. This way the flow channel is not disrupted and the measurements can be taken closer to the turbine inlet section.

Considering all the above, the prototype will be improved for the next experimental campaign in such a manner that it can perform at nominal conditions. Thus, a new material selection will be considered for both stator and rotor blades, as well as design solutions that allow better instrumentation at the inlet and exit sections of the turbine.

However, the experimental turbine can still be used in the current configuration within the limits imposed and it has the advantage of lower manufacturing costs. Thus, it can find its application as an emergency alternative for the TV2-117A power turbine, or it can be used in smaller industrial turboshafts that meet the specified conditions.

## REFERENCES

- [1] Gunston Bill (2006) [1995]. *The Development of Jet and Turbine Aero Engines* (4th ed.). Patrick Stephens Limited. pp. 43–44. ISBN 978-1-85260-618-3.
- [2] Klimov web page (14.11.2022), <https://www.klimov.ru/en/production/helicopter/TV2-117/>
- [3] Zamfirescu V., TV2-117A Free Turbine Turboshaft Engine Description and Maintenance Manual, Engine Maintenance; Documentation and Technical Publications Center: Bucharest, Romania, 1973. (Translation from Romanian)
- [4] Guston Bill. *Jane's Aero-Engines* – Issue Twenty (September 2006), ISSN 1748-2534
- [5] Gunston Bill (1989). *World Encyclopaedia of Aero Engines* (2nd ed.). Cambridge, England: Patrick Stephens Limited. p. 81. ISBN 978-1-85260-163-8
- [6] Varga Bela. *Specific Net Work Or Thermal Cycle Efficiency, One Of The Questions, Engineers Must Face Designing Helicopter Turboshaft Engines*, (2013), <http://hdl.handle.net/20.500.12944/41>
- [7] Catană R.M. et al. *Studies and Experimental Research in the Evaluation of TV2-11A Turboshaft Engine Working Regimes*, Appl. Sci. 2022, <https://doi.org/10.3390/app12073703>
- [8] Advisory Group For Aerospace Research and Development. *Recommended Practices for Measurement of Gas Path Pressures and Temperatures for Performance Assessment of Aircraft Turbine Engines and Components*, Report 245 (1990), ISBN 92-835-0499-2
- [9] The American Society of Mechanical Engineers. *Measurement of Gas Flow by Bellmouth Inlet Flowmeters*, (2011), (ASME MFC-26-2011)
- [10] Froude Hofmann. *Operators Manual for Hydraulic Dynamometer Types Hs125 & HS150 & HS2600*, IM 1205/8, Issue 1 (2007)
- [11] Advisory Group For Aerospace Research and Development. *Suitable Averaging Techniques in Non-Uniform Internal Flows*, Report 182 (1983), ISBN 92-835-1452-1



SPACE TECH EXPO | EUROPE

NOVEMBER 15<sup>TH</sup> - 17<sup>TH</sup> 2022

// Bremen (Germany) //



**The Space Results of COMOTI**  
put ROMANIA in the European Space Orbit!





The only specialized company that integrates  
such activities as

scientific research,  
design,  
manufacturing,  
testing,  
experimental activities,  
technologic transfer and  
innovation

in the field of aircraft and industrial gas turbines and  
high speed bladed machinery.

220D Iuliu Maniu Ave., 061206 Bucharest, ROMANIA,  
P.O. 76, P.O.B. 174

Phone: (+4)021/434.01.98, (+4)021/434.02.31, (+4)021/434.02.40  
Fax: (+4)021/434.02.41, e-mail: [contact@comoti.ro](mailto:contact@comoti.ro)

[www.comoti.ro](http://www.comoti.ro)